CellPress

Structure
Article

Unique Structural Features in DNA Polymerase IV Enable Efficient Bypass of the N^2 Adduct Induced by the Nitrofurazone Antibiotic

Jithesh Kottur,[2,3] Amit Sharma,[2] Kiran R. Gore,[4] Naveen Narayanan,[2,3] Biswajit Samanta,[4] Pushpangadan I. Pradeepkumar,[4,*] and Deepak T. Nair[1,2,*]
[1]Regional Centre for Biotechnology, 180, Udyog Vihar, Phase 1, Gurgaon 122016, India
[2]National Centre for Biological Sciences (NCBS-TIFR), GKVK Campus, Bellary Road, Bangalore 560065, India
[3]Manipal University, Manipal.edu, Madhav Nagar, Manipal 576104, India
[4]Department of Chemistry, Indian Institute of Technology Bombay, Powai, Mumbai 400076, India
*Correspondence: pradeep@chem.iitb.ac.in (P.I.P.), deepak@rcb.res.in (D.T.N.)
http://dx.doi.org/10.1016/j.str.2014.10.019

SUMMARY

The reduction in the efficacy of therapeutic antibiotics represents a global problem of increasing intensity and concern. Nitrofuran antibiotics act primarily through the formation of covalent adducts at the N^2 atom of the deoxyguanosine nucleotide in genomic DNA. These adducts inhibit replicative DNA polymerases (dPols), leading to the death of the prokaryote. N^2-furfuryl-deoxyguanosine (fdG) represents a stable structural analog of the nitrofuran-induced adducts. Unlike other known dPols, DNA polymerase IV (PolIV) from *E. coli* can bypass the fdG adduct accurately with high catalytic efficiency. This property of PolIV is central to its role in reducing the sensitivity of *E. coli* toward nitrofuran antibiotics such as nitrofurazone (NFZ). We present the mechanism used by PolIV to bypass NFZ-induced adducts and thus improve viability of *E. coli* in the presence of NFZ. Our results can be used to develop specific inhibitors of PolIV that may potentiate the activity of nitrofuran antibiotics.

INTRODUCTION

Drug-resistant strains of pathogenic bacteria that exhibit reduced sensitivity to available therapeutic agents are appearing with increasing frequency. The rising incidence of antimicrobial resistance led the government of the United Kingdom to declare in 2013 that this problem "poses a catastrophic threat" (Editorial, 2013; Levy and Marshall, 2004; Taubes, 2008). To enable the development of novel antimicrobials, it is imperative to understand, in fine detail, the strategies used by pathogens to reduce the effectiveness of available antibiotics. Nitrofurans are a family of broad-spectrum antibiotics characterized by the presence of a 5-nitrofuran ring and are effective against both Gram-positive and Gram-negative bacteria. Nitrofurans are activated by cellular enzymes and react with DNA to give rise to N^2 adducts of guanine nucleotides in the genome. This property plays a crucial role in the antibacterial activity of nitrofuran antibiotics (Jarosz et al., 2006; Lu et al., 1979). Nitrofurazone (NFZ) is a representative member of the 5-nitrofuran family of antibiotics and is commercially available in many countries (Figure S1A available online). Topical preparations of NFZ are used to treat skin infections and prevent bacterial infections in burn patients. NFZ-coated catheters are used to prevent urinary tract infections in hospitalized patients (Johnson et al., 2006).

N^2-furfuryl-deoxyguanosine (fdG) represents a stable structural analog of the adduct formed by the action of NFZ (Figure S1B) (Jarosz et al., 2006). The fdG adduct can block replication by high-fidelity DNA polymerases (dPols) such as the Klenow fragment of dPol I from *E. coli* (Jarosz et al., 2006). After every catalytic cycle, replicative dPols check for the presence of a Watson-Crick base pair through formation of noncovalent interactions with the atoms of the minor groove in the newly generated base pair (Johnson and Beese, 2004; Swan et al., 2009). Hence, these polymerases are unable to accommodate minor-groove N^2 adducts in their active sites because of steric clashes between the adducts and the residues that form the floor of the DNA-binding groove. These steric clashes will lead to distortion of the incipient base pair in the active site. Consequently, 3′-OH of the primer, the incoming nucleotide, and the catalytic residues will be misaligned, and therefore, productive catalysis cannot occur.

DNA polymerase IV (PolIV) from *E. coli* belongs to the Y family of dPols and is coded for by the *dinB* gene. PolIV can mediate accurate replication past the fdG adduct (Jarosz et al., 2006, 2009; Shrivastav et al., 2014; Walsh et al., 2012). Consequently, this activity of PolIV reduces the sensitivity of *E. coli* toward the NFZ antibiotic (Jarosz et al., 2006). PolIV can incorporate the correct nucleotide deoxycytidine (dC) opposite this replication-blocking adduct more efficiently than the normal template deoxyguanosine (dG) (Jarosz et al., 2007). In addition, PolIV can also extend from a fdG:dC base pair with very high efficiency (Jarosz et al., 2009). Compared with known translesion dPols, PolIV is unique in its ability to mediate accurate DNA synthesis past N^2-guanine adducts with higher efficiency than on undamaged substrates (Eoff et al., 2010). The mechanistic basis of this superior catalytic efficiency is not known.

To unearth the structural basis of translesion synthesis across the fdG adduct by PolIV, we have determined crystal structures of three functional complexes of PolIV bound to three different DNA duplexes containing the fdG adduct and incoming nucleotide. The three duplexes (Figure S2) possess the fdG adduct at

Table 1. Data Collection and Refinement Statistics

	$PolIV_{fdG:dCMPnPP}$	$PolIV\text{-}fdGT1_{dA:dTMPnPP}$	$PolIV\text{-}fdGT3_{dA:dTMPnPP}$
Data collection			
Wavelength (Å)	0.97926	0.97926	0.97926
Space group	$P2_1$	$P2_1$	$P2_1$
Cell constants (Å) (°)	85.8, 56.8, 112.0	86.5, 57.1, 110.2	85.5, 57.9, 111.0
	90.00, 92.0, 90.00	90.00, 94.8, 90.00	90.00, 90.44, 90.00
Resolution (Å)	2.42 (2.55–2.42)[a]	2.7 (2.75–2.7)[a]	2.18 (2.29–2.18)[a]
R_{sym} or R_{merge}	8.5 (54.0)	7.3 (51.6)	5.8 (32.8)
$I/\delta I$	8.7 (2.3)	17.9 (2.2)	8.9 (3.9)
Completeness (%)	99.9 (99.9)	99.8 (99.2)	99.7 (99.7)
Redundancy	3.7 (3.8)	3.6 (3.6)	3.5 (3.5)
Refinement			
Resolution (Å)	50–2.42	50–2.7	50–2.18
No. of reflections	39,632	28,448	100,627
R_{work}/R_{free}	21.4/26.8	22.5/27.0	21.4/25.8
No. of atoms			
Protein	5,372	5,372	5,376
DNA	1,370	1,383	1,368
dNMPnPP	56	58	58
Ion	4	4	4
Water	105	80	462
Average B factors (Å^2)			
Protein	53.3	61.9	31.6
DNA	55.0	65.4	29.8
$dNMPnPP_{ABCDEK}$	49.8	56.1	22.7
$dNMPnPP_{FGHIJZ}$	28.4	52.1	15.7
Mg^{2+} ions			
A	57.9	61.5	32.0
B	27.2	49.4	7.8
Water	44.5	35.1	29.6
Rmsd			
Bond lengths (Å)	0.004	0.003	0.004
Bond angles (°)	0.994	0.845	0.994

[a]Highest resolution shell is shown in parentheses.

three different positions on the template strand, and the corresponding structures provide snapshots of the PolIV enzyme in the incorporation and extension modes in atomic detail. We have also carried out steady-state kinetic analysis and functional assays for native and mutant versions of PolIV. The structural, biochemical, and functional data presented here highlight the unique features present in PolIV that allow this enzyme to synthesize DNA past the replication-blocking fdG adduct with higher catalytic efficiency than undamaged dG. Overall, the study presents the mechanism used by PolIV to increase the viability of *E. coli* in the presence of the NFZ antibiotic.

RESULTS

Overall Structure

We have determined the structure of three functional complexes of PolIV that provide snapshots of translesion synthesis across the fdG adduct in the incorporation (T_0) and extension (T_1 and T_3) modes (Figure S2). The three complexes $PolIV_{fdG:dCMPnPP}$, $PolIV\text{-}fdGT1_{dA:dTMPnPP}$, and $PolIV\text{-}fdGT3_{dA:dTMPnPP}$ crystallized in the space group $P2_1$ with cell constants of a = 86.7 Å, b = 56.9 Å, c = 111.3 Å, $\alpha = \gamma = 90°$, and $\beta = 94.3°$ (Table 1). In all three structures, the asymmetric unit shows the presence of two complexes. Each complex contains PolIV (1–341 residues), DNA, dNMPnPP, and two Mg^{2+} ions (Figure 1). There is clear electron density visible for the furfuryl moiety of the fdG nucleotide in all three structures (Figure S3).

$PolIV_{fdG:dCMPnPP}$: Incorporation Mode

In the $PolIV_{fdG:dCMPnPP}$ structure, the fdG adduct is at the templating or T_0 position and forms a nascent base pair with the incoming nucleotide dCMPnPP. The template fdG nucleotide interacts with residues of the fingers (I31, R38, V40, S42, and A56) and palm (F76) domains (Figure S4). In addition, residues from the polymerase-associated domain (PAD) region (T248, F295, and R330) also interact with the fdG nucleotide. The incoming

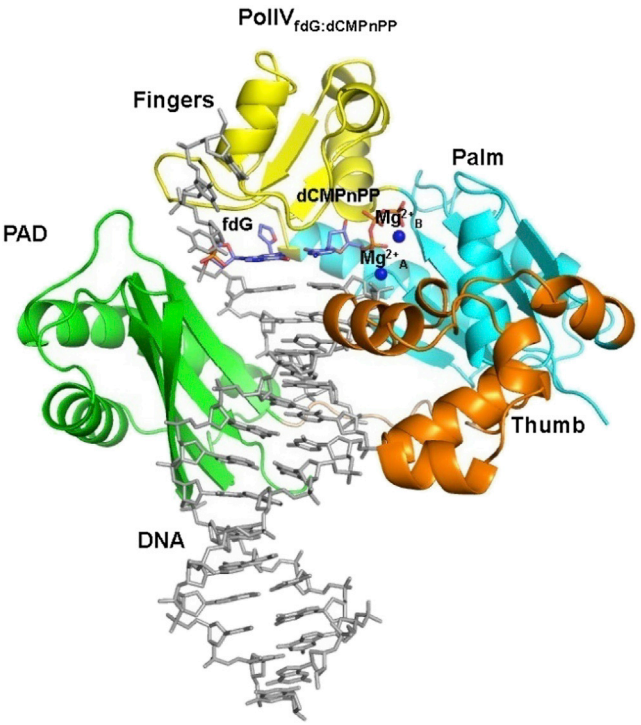

Figure 1. Structure of the PolIV$_{fdG:dCMPnPP}$ Complex
The structure of PolIV is displayed in ribbon representation with the palm, fingers, and thumb domains and the PAD region colored cyan, yellow, orange, and green, respectively. DNA is displayed in stick representation, and atoms are colored gray. The template fdG and incoming dCMPnPP are colored according to element. The magnesium ions are shown as blue spheres.

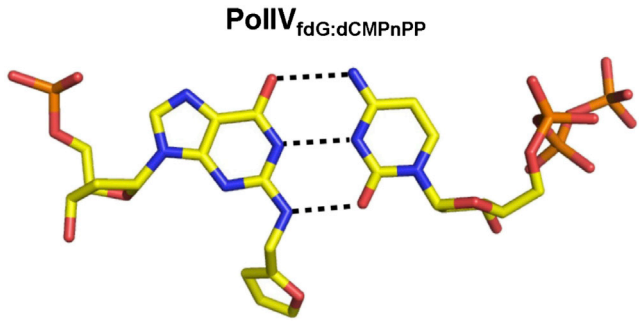

Figure 2. fdG:dCMPnPP Base Pair: Incorporation Mode
The incipient base pair in the PolIV active site is displayed. The template fdG and incoming dCMPnPP are colored according to element and displayed in stick representation.

nucleotide dCMPnPP is proximal to residues of the palm (D8, M9, D10, D103, E104, and K157) and fingers (C11, F12, F13, S42, T43, R49, and S55) domains.

The structure of PolIV with undamaged substrate DNA with dG at the T_0 position paired with dCMPnPP (PolIV$_{dG:dCMPnPP}$) is available (Protein Data Bank [PDB] accession number 4IRC) (Sharma et al., 2013). The PolIV$_{fdG:dCMPnPP}$ superimposes onto the PolIV$_{dG:dCMPnPP}$ structure with an rmsd value of 0.4 Å (341 Cα pairs). In addition, the conformation of the residues that interact with the template and incoming nucleotides exhibit only marginal differences in the two structures (Figure S5). The Mg^{2+} ions are located at identical locations, and there is no difference in the conformation of the catalytic residues between the two structures. The base moiety of fdG forms three hydrogen bonds with the Watson-Crick edge of the cytosine base of incoming dCMPnPP (Figure 2). The C1′-C1′ distance for the fdG:dCMPnPP base pair is 10.6 Å and is comparable with that observed for dG:dC Watson-Crick base pair (10.7 Å). Overall, the comparison of the two structures shows that the PolIV enzyme can accommodate fdG adduct with minimal change in structure. The furfuryl moiety of fdG is oriented toward the minor groove and is located in an elongated channel that is formed between the fingers domain and the PAD region (Figure 3).

The archaeal homolog of PolIV, Dpo4 (27% sequence identity), exhibits considerably lower ability to incorporate deoxycytidine triphosphate (dCTP) opposite fdG (Figure S6A). The structures of Dpo4 in complex with undamaged DNA with a nascent dG:dCTP base pair in the active site (PDB accession number 2ATL) and in complex with DNA containing different N^2 adducts are available (Bauer et al., 2007; Rechkoblit et al., 2006; Xu et al., 2009; Zang et al., 2005; Zhang et al., 2009a, 2009b; Zhang and Guengerich, 2010; Zhao et al., 2012a). The alignment of the PolIV$_{fdG:dCMPnPP}$ with 2ATL through superimposition of the palm residues showed that there were differences in the relative orientation of the different domains of PolIV and Dpo4 (Figure 4A). Consequently, there are significant differences in the orientation of substrate DNA in the DNA-binding grooves of the two enzymes (Figure 4A). In Dpo4, the orientation of DNA on the enzyme is such that the template nucleotide (Figures 4B and 4C) is present close to the enzyme surface (see also Supplemental Results).

The PolIV$_{fdG:dCMPnPP}$ structure shows that the furfuryl moiety is present in a cavity located in a hydrophobic patch present at the junction of the fingers and palm domains. This region is formed by the residues F13, I31, G32, G33, L71, L72, P73, G74, F76, and Y79 (Figure 5). In the case of PolIV, the mutations F13→V and Y79→L have been shown to compromise the ability of this enzyme to bypass fdG (Jarosz et al., 2006, 2009). In addition, mutation of the residues F12, F13, and Y79 enhances the sensitivity of *E. coli* toward NFZ (Benson et al., 2011; Jarosz et al., 2006). Thus, perturbation of the hydrophobic patch surrounding the cavity occupied by the furfuryl moiety compromises the ability of PolIV to bypass the fdG adduct.

The S42 residue is present close to the midline of the fdG:dCMPnPP base pair toward the minor groove (Figure 6A). This residue forms hydrogen bonds with the N^2 atom of template fdG, O2 atom of incoming dCMPnPP and with the oxygen atom of the furfuryl moiety. The interactions formed by S42 stabilize the fdG adduct and the dCMPnPP nucleotide in the correct orientation to ensure productive base pairing that is compatible with catalysis.

To validate the role of the S42 residue in translesion synthesis across fdG, the ability of mutant PolIV (S42→A) to incorporate dCTP opposite this adduct was assessed. Steady-state kinetic experiments showed that the catalytic efficiency (k_{cat}/K_m) for incorporation of dCTP opposite fdG decreases 2.3-fold from 1,150 $mM^{-1}min^{-1}$ for wild-type (WT) PolIV (wtPolIV) to 500 $mM^{-1}min^{-1}$ for the S42→A mutant (Table 2). In comparison,

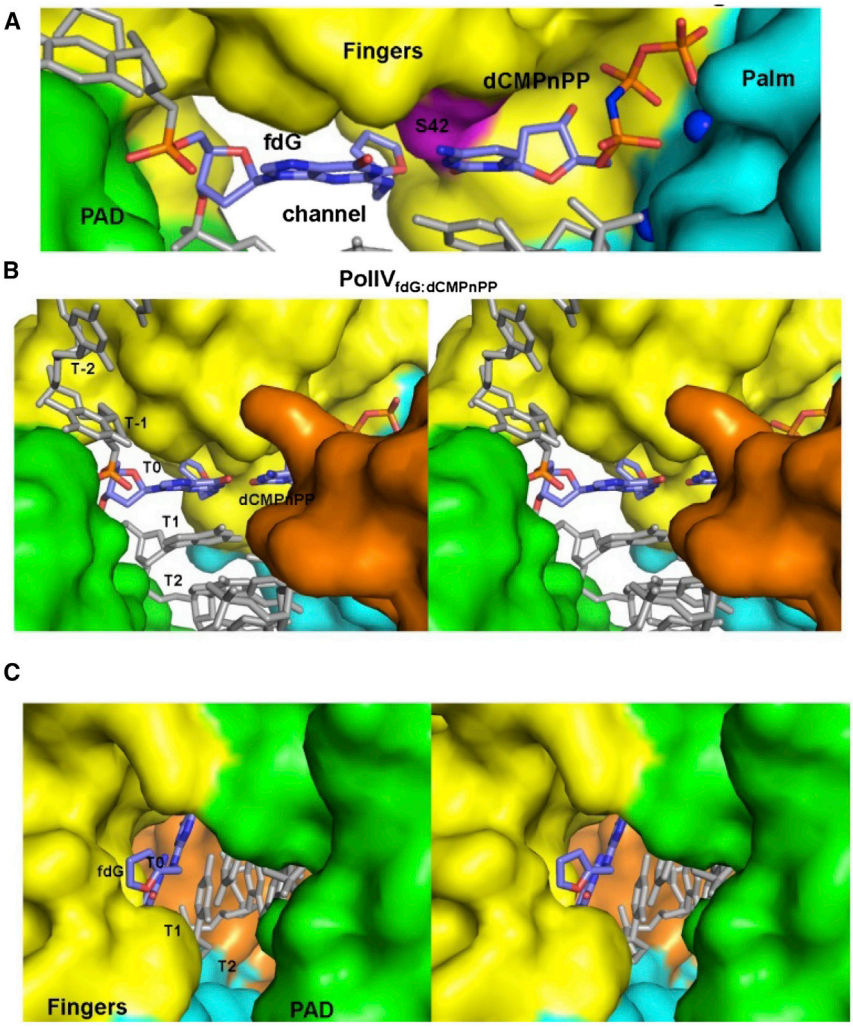

Figure 3. Structure of PolIV Bypassing the fdG Adduct: Incorporation Mode—PolIV$_{dG:dCMPnPP}$

(A) The surface of PolIV is displayed with the palm, fingers, and PAD region colored cyan, yellow, and green, respectively. The DNA and dCMPnPP are displayed in stick representation, and Mg^{2+} ions are shown as blue spheres. The thumb domain has been removed to show the fdG:dCMPnPP base pair clearly. The atoms of the incipient base pair are colored according to element, and the surface of S42 residue is shown in magenta.

(B and C) Stereo figures of the active site of PolIV$_{fdG:dCMPnPP}$ as viewed from the top (B) and bottom (C) are displayed. In (B), the surface of the thumb domain is displayed in orange color.

The pictures show that the furfuryl group is present in a channel formed between the fingers domain and PAD regions when fdG is present in the T_0 position.

the k_{cat}/K_m values for incorporation of dCTP by WT and mutant PolIV opposite undamaged dG are nearly identical. These experiments show that S42 residue is important for optimal activity.

We also assessed the contribution of the S42 residue in reducing sensitivity of *E. coli* toward the NFZ antibiotic. This assay estimated the viability of *E. coli* in the presence of NFZ when WT and mutated PolIV were expressed ectopically from a plasmid in a strain wherein the *dinB* gene had been deleted. Transformation with a plasmid bearing the WT *dinB* gene resulted in about 2.5-fold more colonies than mutant (S42→A) *dinB* (Figure 6B). This observation is consistent with the inference that the S42 residue of PolIV plays an important role in translesion DNA synthesis across the fdG adduct.

PolIV-fdGT1$_{dA:dTMPnPP}$: Extension Mode 1

In the PolIV-fdGT1$_{dA:dTMPnPP}$ structure, the fdG nucleotide is present at the T1 position (Figure S2) and paired with dC present at the 3′ terminus of the primer (Figure 7). This base pair represents the state of the incipient fdG:dCTP (as visualized in the PolIV$_{fdG:dCMPnPP}$ structure) after one round of replication. The fdG nucleotide forms a base pair with the dC residue, and the C1′-C1′ distance for this base pair is the same as that observed in the PolIV$_{fdG:dCMPnPP}$ (Figure 7A). Thus, this base pair does not undergo any structural distortion as it translocates from the T_0 position in the active site to the T_1 position in double-stranded DNA (dsDNA). The furfuryl moiety in this base pair is located in the extended channel formed between the fingers domain and PAD region (Figures 7B and 7C). This moiety is at least 5.0 Å away from any atom of the PolIV enzyme. The fdG adduct does not clash with any atom of the enzyme and hence does not interfere with productive catalysis during extension.

In the PolIV-fdGT1$_{dA:dTMPnPP}$ structure, the incipient base pair in the active site is dA:dTMPnPP. The structure of PolIV-fdGT1$_{dA:dTMPnPP}$ superimposes onto the structure of the PolIV$_{dA:dTMPnPP}$ (PDB accession number 4IR1) structure with an rmsd of 0.5 Å. There is no change in the conformation of the dA:dTMPnPP base pair, the catalytic residues, the position of 3′-OH on the primer, and the location of the catalytic Mg^{2+} ions.

PolIV-fdGT3$_{dA:dTMPnPP}$: Extension Mode 2

The fdG nucleotide is located at the T_3 position (Figure S2) in the PolIV-fdGT3$_{dA:dTMPnPP}$ structure (Figure 8). This fdG:dC base pair in this structure represents the state of the incipient fdG:dCTP after three rounds of replication. The C1′-C1′ distance for the fdG:dC base pair is the same as that seen in the PolIV$_{fdG:dCMPnPP}$ (Figure 8A).

In this position, the furfuryl moiety adopts a conformation such that it is located within the minor groove and does not extrude out of the double helix. Because of the orientation in which the thumb domain interacts with DNA, there is a large cavity formed between the bottom half of the thumb, palm and substrate DNA (Figure 8B). The furfuryl moiety also points toward this cavity and is therefore located at least 6 Å away from the atoms of the protein. Overall, the relative orientation of the palm and thumb domains and the conformation adopted by the furfuryl moiety

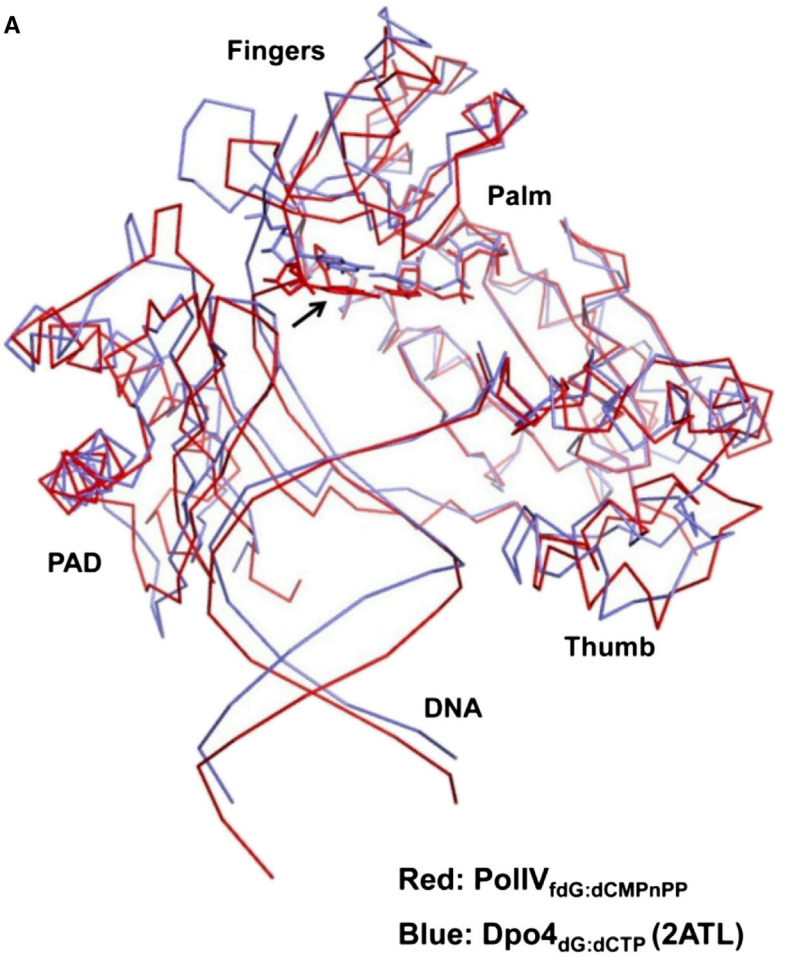

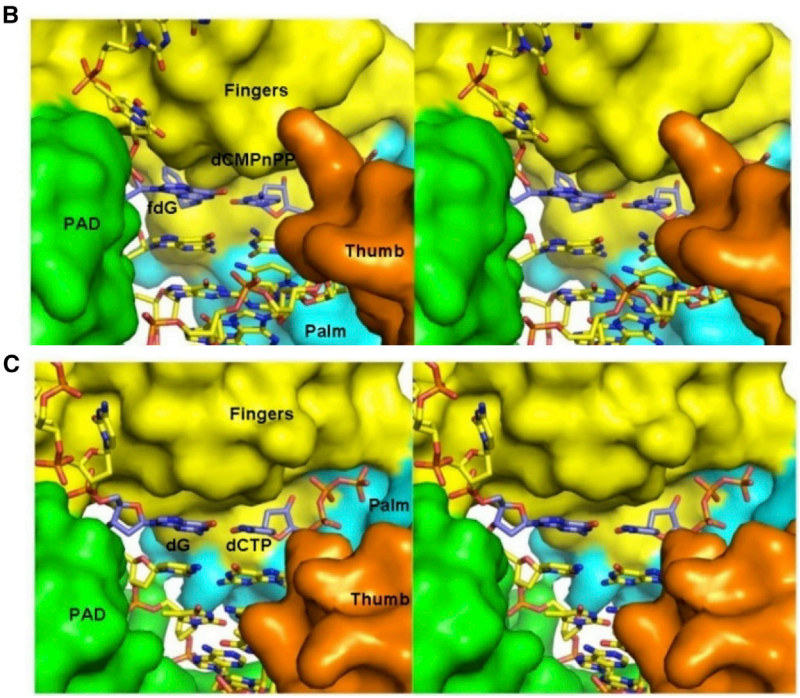

Figure 4. Comparison of the Structure of the PolIV$_{fdG:dCMPnPP}$ Complex with that of Dpo4 Bound to DNA Presenting Template dG: PDB 2ATL

(A) The alignment of the two structures through superimposition of the palm residues highlights the differences in the relative orientation of domains and substrate DNA in the two structures. The backbone trace of protein and DNA in PolIV$_{fdG:dCMPnPP}$ and Dpo4$_{dG:dCTP}$ are shown in red and blue, respectively. The nascent base pair in both structures is displayed in stick representation and marked by an arrow to highlight the difference in their positioning with respect to the different domains.

(B and C) A close-up of the active site is shown in stereo for the PolIV$_{fdG:dCMPnPP}$ complex (B) and Dpo4$_{dG:dCTP}$ (C) to highlight the differences in surface topology in the area close to the minor groove of the template nucleotide.

The palm, fingers, and thumb domains and the PAD region are colored as in Figure 3. The DNA and dCMPnPP/dCTP are shown in stick representation and colored according to element.

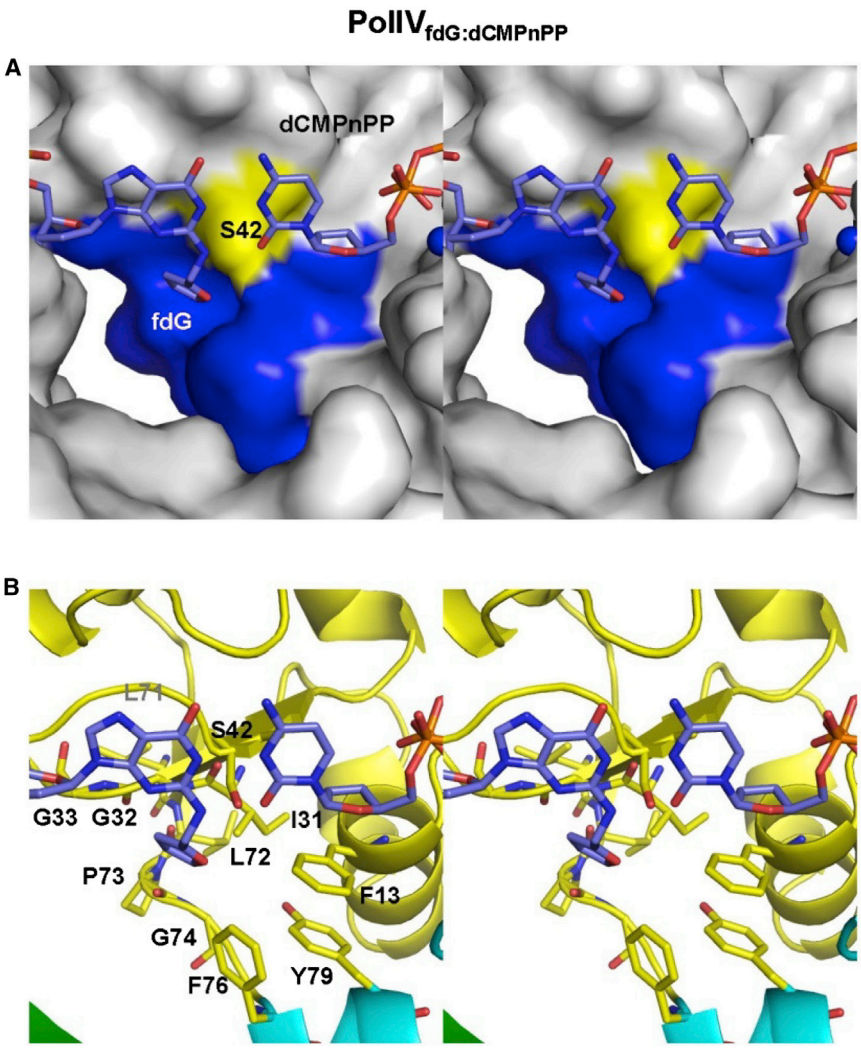

Figure 5. Residues Lining the Furfuryl Moiety in PolIV$_{fdG:dCMPnPP}$

The furfuryl moiety of fdG is present close to a hydrophobic patch formed by the side chains of F13, I31, L72, F76, and Y79 and backbone atoms of G32, G33, P73, and L71. The furfuryl moiety is present in a cavity located in this hydrophobic patch.

(A and B) Stereo figures wherein the surface formed by these residues is displayed (A) or the residues are shown in stick representation (B). The hydrophobic patch in (A) is colored in blue, and the surface corresponding to S42 is colored in yellow.

ensure that there are no steric clashes between the fdG adduct and atoms of PolIV.

The incipient base pair in the PolIV-fdGT3$_{dA:dTMPnPP}$ structure is again dA:dTMPnPP. As in the case of PolIV-fdGT1$_{dA:dTMPnPP}$, the location of the catalytic ions and the 3′-OH of the primer do not exhibit any difference compared to the PolIV$_{dA:dTMPnPP}$ structure. In addition, the conformation of the catalytic residues is identical to that seen in the PolIV$_{dA:dTMPnPP}$ structure. Overall, the presence of the furfuryl moiety at the T_3 position has no effect on the structure of the incipient base pair, catalytic residues, and catalytic ions.

The three structures PolIV$_{fdG:dCMPnPP}$, PolIV-fdGT1$_{dA:dTMPnPP}$, and PolIV-fdGT3$_{dA:dTMPnPP}$ superimpose onto one another with rmsd values of about 0.5 Å. The PolIV$_{fdG:dCMPnPP}$ superimposes onto the PolIV$_{dG:dCMPnPP}$ (PDB accession number 4IRC) structure with an rmsd value of 0.4 Å (341 Cα pairs). Additionally, the two extension mode structures PolIV-fdGT1$_{dA:dTMPnPP}$ (PDB accession number 4IR1) and PolIV-fdGT3$_{dA:dTMPnPP}$ superimpose onto the structure of the PolIV$_{dA:dTMPnPP}$ complex with rmsd values of 0.5 and 0.3 Å, respectively. This comparison shows that there is minimal change in the structure of PolIV as it synthesizes DNA past the fdG adduct.

DISCUSSION

DNA lesions are formed by the action of a variety of genotoxic agents that react with different atoms on different nucleotides. The N^2 atom of the guanine base is particularly vulnerable to modification by a number of chemical agents.(Dipple, 1995). The consequent minor-groove adducts may be mutagenic or block replication, and therefore, their presence can be lethal to the cell. The known translesion dPols exhibit varying ability to bypass different N^2 adducts.

The eukaryotic Y family dPols ι, η, κ, and Rev1 can incorporate nucleotides opposite N^2-adducted guanines (Choi and Guengerich, 2008; Choi et al., 2006c; Minko et al., 2001; Pence et al., 2009, 2011; Perrino et al., 2005; Suzuki et al., 2002; Washington et al., 2004; Wolfle et al., 2006; Yasui et al., 2008; Zhang et al., 2002; Zhao et al., 2012b). Polι, Polη, and Rev1 use distinct strategies to synthesize DNA on damaged and undamaged DNA substrates (Biertümpfel et al., 2010; Nair et al., 2004, 2005; Pence et al., 2009; Silverstein et al., 2010a). In Polι, a Lys residue constricts the active site and ensures that the template guanine has to rotate from anti to syn conformation for stable base pairing, and thus the N^2 atom is oriented toward the major groove. In the case of Rev1, the template nucleotide is flipped out of the active site, and the identity of the correct incoming nucleotide dCTP is determined by an Arg residue. Polη possesses an unusually open active site that allows it to stabilize damaged template nucleotides and normal incoming nucleotide triphosphates in a Watson-Crick configuration (Biertümpfel et al., 2010; Silverstein et al., 2010b). These strategies lead to a loss in the catalytic efficiency of nucleotide incorporation opposite N^2-adducted guanines, can be mutagenic, and also may require the presence of an extender dPol (such as Polκ or Polζ) to complete translesion bypass (Choi and Guengerich, 2006; Choi et al., 2006c; Eoff et al., 2010; Nair et al., 2006; Washington et al., 2004; Zhang et al., 2002; Zhao et al., 2006, 2012b). Polη has been shown to carry out mutagenic bypass of the different N^2 adducts of dG (Choi and Guengerich, 2005; Choi et al., 2006b; Minko et al., 2001; Yasui et al., 2008; Zhao

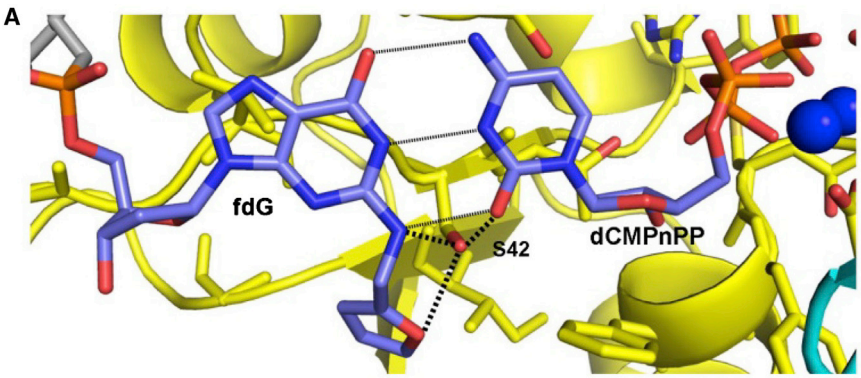

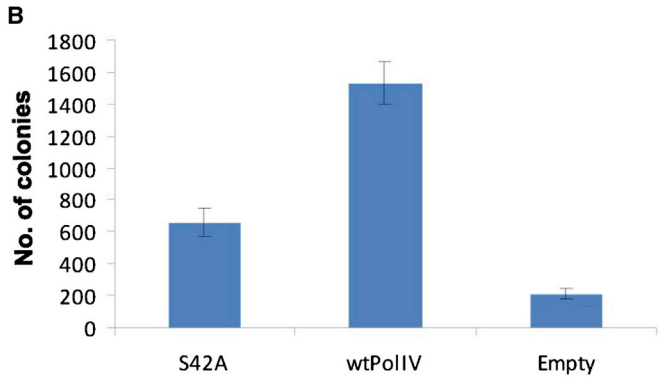

Figure 6. Role of S42 Residue in fdG Bypass

(A) The incipient fdG:dCMPnPP base pair in the $PolIV_{fdG:dCMPnPP}$ structure is displayed in stick representation. The hydrogen bonds formed between (i) S42 and fdG (ii) S42 and dCMPnPP and (iii) fdG and dCMPnPP are highlighted by dotted lines.

(B) Growth assay to assess the role of S42 in reducing sensitivity of *E. coli* toward NFZ. The bar graph displays the number of colonies obtained in media containing NFZ (4 μg/ml) for a *dinB*-deleted strain, dinB749(del)::kan, transformed with plasmids bearing the WT (pDJNNwtdb) and mutated dinB gene (pDJNNSER42ALAdb) and with empty vector.

Error bars represent SD (n = 3).

et al., 2006, 2012b). All known translesion dPols generally exhibit reduced catalytic efficiency during DNA synthesis past DNA lesions (Eoff et al., 2010).

The present study shows that PolIV possesses structural features that allow it to mediate efficient and error-free translesion synthesis past the fdG adduct. The extended channel between the PAD and fingers domains provides space that prevents N^2 adducts from clashing with atoms that form the enzyme surface. In addition, the cavity present in the hydrophobic patch toward the minor groove and the S42 residue stabilize the fdG adduct in the active site in a conformation compatible with productive catalysis. The stacking and H-bonding interactions formed between the furfuryl group with the hydrophobic patch and the S42 residue, respectively, are absent in the case of template dG. Therefore, the fdG adduct is stabilized better in the active site of PolIV than undamaged dG. Consequently, PolIV can incorporate dCTP opposite fdG with higher catalytic efficiency than opposite template dG.

The finger-PAD channel and the large cavity formed between DNA and the thumb domain will ensure that extension from the fdG:dCTP base pair occurs unhindered. The space provided by the finger-PAD channel and the thumb cavity will prevent steric clashes between fdG and residues of PolIV during incorporation and extension. Overall, on binding substrate DNA, the relative orientation of the different domains of PolIV is such that the channels and cavities are formed that can accommodate fdG adduct during incorporation and extension. Consequently, there are no steric clashes between atoms of the adduct and the residues that form the enzyme surface. As a result, the fdG adduct can reside in the PolIV active site and DNA-binding groove during incorporation and extension without any distortion in the structure of enzyme and substrate. Because there is no change in the alignment of atoms of the catalytic residues, 3′-OH of the primer, incoming and template nucleotides and cofactor ion, PolIV can mediate accurate translesion synthesis past the fdG adduct with high catalytic efficiency. Overall, unique structural and active-site features present in PolIV enable it to rescue replication stalled at the fdG adduct and thus prevent death of the organism. Consequently, the activity of PolIV results in reduction in the sensitivity of *E. coli* toward nitrofuran antibiotics such as NFZ.

PolIV has also been shown to accurately bypass other N^2 adducts, such as the benzo[*a*]pyrene-7,8-diol 9,10-epoxide dG (BPDE-N^2-dG), N^2-(1-carboxyethyl)-2′-dG, and 2-tetrahydrofuran-2-yl-methylguanine adducts (Seo et al., 2006; Shen et al., 2002; Shrivastav et al., 2014; Yuan et al., 2008). In addition, PolIV has been shown to mediate efficient recovery of replication forks stalled at N^2 adducts (Ikeda et al., 2014). The structural attributes of PolIV that facilitate efficient and accurate bypass past fdG should also enable translesion synthesis past these and other N^2 adducts of varying size and chemical nature.

The archaeal homolog of PolIV, Dpo4 (*Sulfolobus solfataricus*) exhibits varying reduction in catalytic efficiency during bypass of N^2 adducts of different sizes (Bauer et al., 2007; Zhang et al.,

Table 2. Catalytic Efficiency of WT and Mutant PolIV

	Template fdG		Template dG	
	wtPolIV	S42A	wtPolIV	S42A
K_M for dCTP (μM)	0.33 ± 0.06	0.30 ± 0.06	1.01 ± 0.15	0.47 ± 0.08
k_{cat}/K_M ($mM^{-1}min^{-1}$)	1,150	500	280	240

K_M values are expressed as mean ± SD (n = 3).

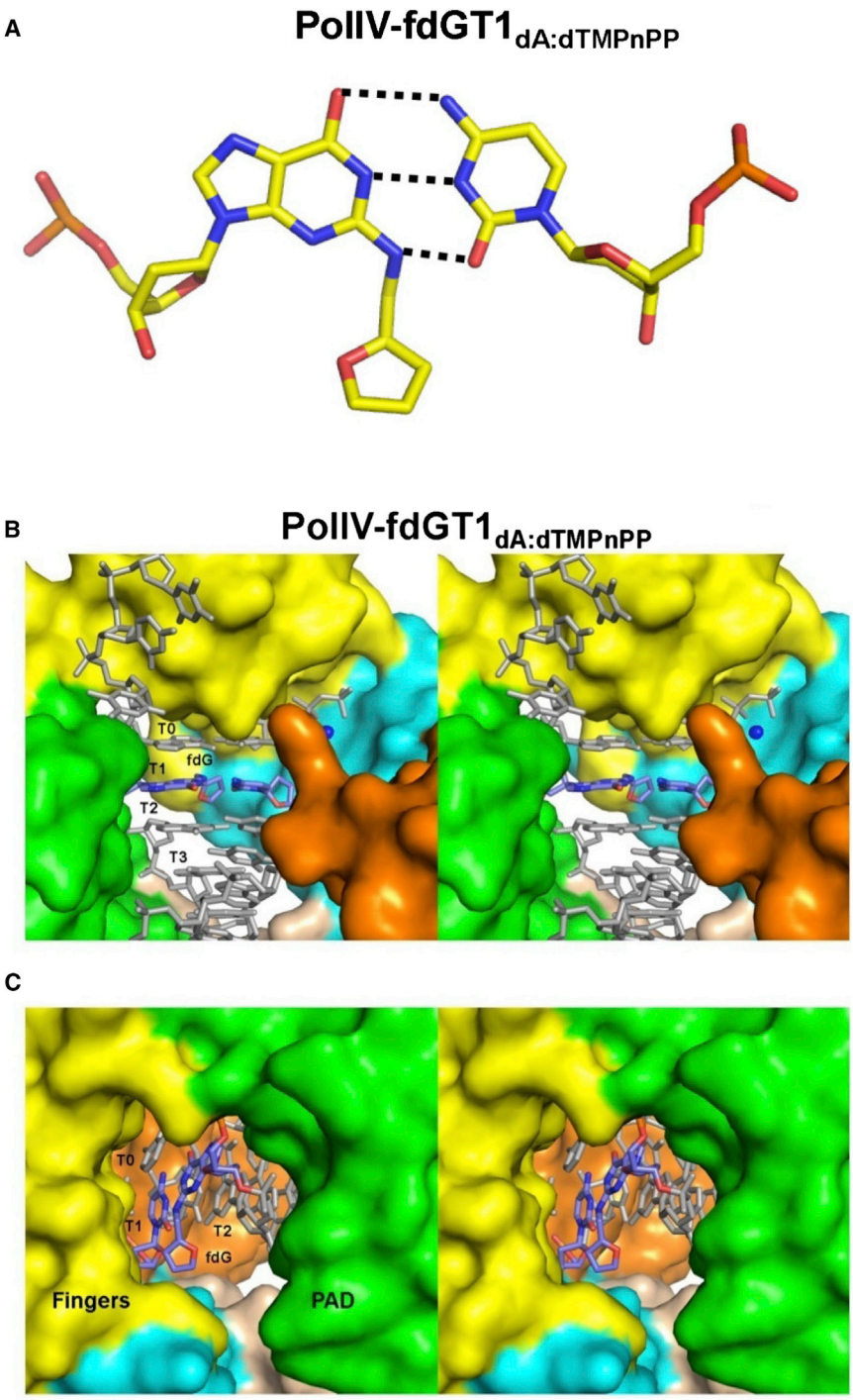

Figure 7. Structures of PolIV Bypassing the fdG Adduct: Extension Mode 1

(A) fdG:dC base pair. The first base pair in the double-stranded region of substrate DNA in the PolIV-fdGT1$_{dA:dTMPnPP}$ structure is shown. The template fdG and incoming dCMPnPP are colored according to element and displayed in stick representation.

(B and C) Stereo figures of the active site of PolIV-fdGT1$_{dA:dTMPnPP}$. In (B), the active site is viewed from the top, and in (C), the active site is shown from the bottom. The surface of PolIV is displayed with the different domains colored as in Figure 3. DNA and dCMPnPP are displayed in stick representation, and Mg^{2+} ions are shown as blue spheres. The figure shows that the furfuryl group is present in a channel formed between the fingers domain and PAD regions when fdG is present in the T_1 position.

2009b; Zhang and Guengerich, 2010). In the case of some N^2 adducts, such as N^2,N^2-dimethyl dG, bypass by Dpo4 is mutagenic (Bauer et al., 2007; Zang et al., 2005; Zhang et al., 2009a, 2009b; Zhao et al., 2012a). Also, a mixture of conformations was seen for the adducted template nucleotide during nucleotide incorporation opposite different bulky N^2 adducts of dG (Chandani and Loechler, 2007; Xu et al., 2009; Zhang et al., 2009b). The comparison of PolIV and Dpo4 shows that each enzyme exhibits a unique relative orientation of the different domains and the orientation of substrate DNA in the DNA-binding groove. In the case of Dpo4, the template nucleotide is present closer to the fingers domain such that bulky N^2 adducts of dG will clash with the enzyme surface. In addition, the cavity occupied by the furfuryl moiety in the hydrophobic patch present toward the minor groove of the incipient base pair in PolIV is absent in Dpo4. Also, an alanine residue is present in the position equivalent to S42 of PolIV, and the stabilizing interactions formed between S42 and the nascent base pair will not exist in the case of Dpo4. Overall, there are differences in the relative orientation of the domains, orientation of DNA in the active-site groove, and surface features close to the template nucleotide. As a result of these differences, in the case of Dpo4, N^2 adducts with exocyclic rings toward the minor groove may clash with the enzyme surface and consequently lead to structural distortions in substrate DNA and heterogeneity in the conformation of the template nucleotide. This will result in the misalignment of the substrates (DNA, deoxynucleotide triphosphate), cofactor (Mg^{2+} ions), and catalytic residues of the enzyme. The misalignment will lead to a loss in catalytic efficiency and decrease the ability of Dpo4 to bypass N^2 adducts. Overall, the comparison of PolIV with Dpo4 shows that subtle differences in the relative orientation of different domains and the presence or absence of specific residues at key locations in the active site can lead to drastic differences in the lesion-bypass properties of Y family dPols.

PolIV is known to participate in stress-induced mutagenesis through error-prone DNA synthesis on undamaged DNA (Foster, 2007; Galhardo et al., 2007; Nohmi, 2006). This property of PolIV

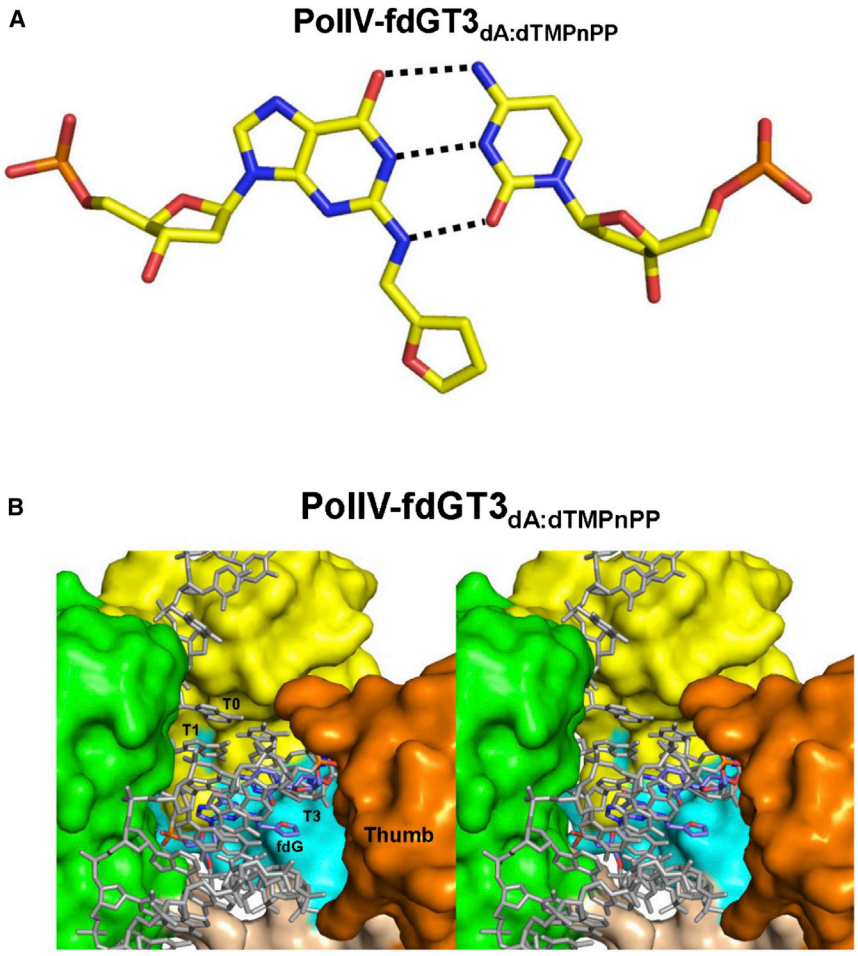

Figure 8. Structure of PolIV Bypassing the fdG Adduct: Extension Mode 2

(A) The third base pair in the double-stranded region of substrate DNA in the PolIV-fdGT3$_{dA:dTMPnPP}$ structure is shown, with template fdG and incoming dCMPnPP colored according to element and displayed in stick representation.

(B) Stereo figures of the DNA-binding groove of PolIV-fdGT3$_{dA:dTMPnPP}$, with surfaces of different domains of PolIV colored as in Figure 3. DNA and dCMPnPP are displayed in stick representation, with atoms of the fdG:dC base pair are colored according to element. In the T_3 position, the furfuryl moiety is oriented toward a cavity formed between the palm and thumb domains and DNA.

aids in the appearance of mutations that can alleviate selection pressure imposed by an adverse environment. The S42 residue has been shown to play an important role in the mutator activity of PolIV and probably ensures that the mutator activity is calibrated in the right range: not too high to compromise genetic viability and not too low to avoid presenting an inadequate number of genomic templates for natural selection. The same residue also plays an important role in stabilizing N^2 adducts in the active site in an orientation compatible with catalysis. Overall, PolIV possesses unique structural attributes that allow it to bypass N^2 adducts with higher catalytic efficiency than undamaged DNA and also carry out error-prone DNA synthesis on undamaged DNA. These unique properties of PolIV may allow prokaryotic organisms to couple tolerance of DNA damage with calibrated mutagenesis. The effect of baseline levels of DNA damage, in the form of N^2 adducts, on DNA replication can be neutralized by PolIV because of its ability to bypass N^2 adducts accurately, and subsequently the damaged nucleotides can be removed by the nucleotide excision repair pathway. However, as the number of damaged nucleotides increases, the continual recruitment and activity of PolIV on these multiple sites will lead to an increasing number of mutations in undamaged DNA. Thus, the activity of PolIV will ensure that if the challenge to genetic integrity crosses a critical magnitude, then the organism is endowed with an ability to evolve and relieve selection pressure imposed by a stressful environment to ensure survival of the organism.

Polκ is the only eukaryotic homolog that possesses a serine residue at a position equivalent to S42 (S137) in PolIV. This enzyme possesses a unique substructure at the N terminus, termed the N clasp, that allows it to encircle substrate DNA and accommodate a Watson-Crick base pair in its spacious active site (Lone et al., 2007). Polκ has been shown to bypass N^2 adducts, including fdG, accurately (Choi et al., 2006a; Jarosz et al., 2006; Jia et al., 2008; Suzuki et al., 2002; Yasui et al., 2006). A recent study on mouse Polκ suggests that the equivalent of the finger-PAD channel plays a critical role in the ability of the enzyme to bypass the BPDE-N^2-dG adduct (Liu et al., 2014). The S137 residue in the active site of Polκ may also play an important role in bypass of N^2 adducts by this dPol.

Our study highlights the mechanism used by PolIV to reduce the sensitivity of *E. coli* toward the NFZ antibiotic. NFZ belongs to the 5-nitrofuran family of antibiotics, and new members of this family may be used as drugs against multidrug resistant bacteria, trypanosomes, and nosocomial pathogens (Bot et al., 2013; Tangallapally et al., 2007; Zorzi et al., 2014). It has been suggested that members of this family of antibiotics may have a common mode of action, and therefore PolIV may play a role in reducing the sensitivity of prokaryotes to these new members of the 5-nitrofuran family also through translesion bypass of the DNA adducts formed by the action of these antibiotics (Ryan et al., 2011). In addition, the mutator activity of PolIV has been implicated in the appearance of mutations that provide resistance to antibiotics (Cirz and Romesberg, 2006; Foster, 2007; Galhardo et al., 2007; Nohmi, 2006; Petrosino et al., 2009). A number of orthologs of PolIV from different pathogenic bacteria exhibit very high homology (~66% identity), suggesting that the observed functions of PolIV will be conserved in the corresponding organisms (Figure S8). Hence, inhibition of the activity of orthologs of PolIV will enhance the sensitivity of pathogenic bacteria toward nitrofuran antibiotics such as NFZ and also reduce the probability of the appearance of adaptive mutations that

render resistance toward therapeutic agents. Overall, perturbing the mutator and translesion activities of Y family dPols may represent an effective strategy to combat the rising incidence of multidrug resistance in pathogenic strains of bacteria.

EXPERIMENTAL PROCEDURES

Oligonucleotides, Protein Purification, and Crystallization

Phosphoramidite of fdG was synthesized and used to assemble different oligonucleotides using the Mermade 4 solid-phase synthesizer (Gore et al., 2013). Then 50-mer and 18-mer oligonucleotides were synthesized for primer extension assays and crystallization, respectively. All the modified oligonucleotides were PAGE purified (20%, 8 M urea), and the presence of the fdG adducts in these oligonucleotides was confirmed by MALDI or electrospray ionization (ESI) mass spectrometry. PolIV was purified to high homogeneity as described previously (Sharma et al., 2013). The ternary complexes for crystallization were reconstituted by mixing PolIV (0.3 mM) with dsDNA (0.36 mM) followed by addition of 5 mM dNMPnPP (Jena Biosciences) and 5 mM $MgCl_2$. After screening and optimization, the best crystals were obtained in 0.1 M acetate (pH 4.8), 5% to 12% w/v 2-methyl-2,4-pentanediol.

Structure Determination and Crystallographic Refinement

X-ray diffraction data were collected at PXIII beamline of Swiss Light Source (SLS) ($PolIV_{fdG:dCMPnPP}$ and PolIV-$fdGT3_{dA:dTMPnPP}$) and BM14 beamline of the European Synchrotron Radiation Facility (ESRF) (PolIV-$fdGT1_{dA:dTMPnPP}$). All data were processed using iMosflm and SCALA in CCP4 (Leslie and Powell, 2007). Using PHASER, the structure of the $PolIV_{fdG:dCMPnPP}$ was determined using $PolIV_{dG:dCMPnPP}$ (PDB accession number 4IRC) as a search model (McCoy et al., 2007; Sharma et al., 2013). For PolIV-$fdGT1_{dA:dTMPnPP}$ and PolIV-$fdGT3_{dA:dTMPnPP}$, the structures were determined using that of $PolIV_{dA:dTMPnPP}$ (PDB accession number 4IR1) as a search model.

Using CNS, a round of rigid-body, b-factor, and positional refinement was carried out followed by calculation of 2fo-fc and fo-fc maps (Brünger et al., 1998). These maps showed the presence of density corresponding to the fdG adduct (Figure S3). The coordinates for the fdG adduct were built manually and subsequent refinement was carried out in PHENIX until convergence (Adams et al., 2010). The data and refinement statistics are provided in Table 1. The majority of the residues are in the favorable regions of the Ramachandran plot, with only 1% of residues in the disallowed regions. The structures were analyzed using PyMOL (Schroedinger) and CCP4i. Figures were generated using PyMOL.

Steady-State Kinetic Assays with WT and Mutant PolIV

The S42A mutant of PolIV was prepared previously and purified as previously described (Sharma et al., 2013). The oligonucleotides used for primer extension assays were CCTACCGTGCCTACCTGAACAGCTGGTCACACT(fdG)ATGCC TACGAGTACG (template) and CGTACTCGTAGGCAT (primer). The primer has a 6-FAM label at the 5′-end. For primer extension assay, the reaction mixture (20 μl) consisted of 5 μM dCTP, 40 nM DNA substrate, 0.1 mM ammonium sulfate, 50 μg/ml BSA, 2.5 mM $MgCl_2$, 4 μl 5X assay buffer (125 mM Tris-Cl [pH 8.0] and 5 mM dithiothreitol) and 4 nM of PolIV (WT or mutant). The reaction was carried out for varying times (30 s to 30 min) at 37°C and terminated by adding 10 μl of stop solution (80% formamide, 1 mg/ml xylene cyanol, 1 mg/ml bromophenol blue, and 20 mM EDTA) followed by 2 min of incubation at 95°C. This mixture was cooled on ice for 10 min. Fifteen microliters of this sample was loaded onto a 20% polyacrylamide gel containing 8 M urea and 1X Tris-borate-EDTA to resolve the reaction products. Resolved products on the gel were observed by excitation at 488 nm using the Biorad Pharos FX Plus Molecular Imager. The intensities of the observed bands were quantified using Quantity one, 1D analysis software. The level of incorporation was calculated using the following equation:

$$\text{Percentage incorporation} = \frac{\text{Is}}{(\text{Is} + \text{Ip})} \times 100,$$

where Is is the intensity of extended primer, and Ip is the intensity of the intact primer band in the same lane.

The time point at which 20% of the primer had been extended was used for further analysis. Reactions were carried out with varying concentration of incoming dCTP. After quantification of the resolved products, apparent K_m and V_{max} values were calculated using a Lineweaver-Burk plot as previously described (Sharma and Nair, 2012).

In Vivo Growth Assay with WT and Mutated *dinB*

For the sensitivity assay, the *dinB*-deleted strain, dinB749(del)::kan, was obtained from the Coli Genetic Stock Centre (Yale University). Freshly prepared competent cells of this strain were transformed with empty vector and plasmids bearing WT and mutated (S42A) *dinB* genes. Overnight cultures of these transformants were used to inoculate (at 1:1000 dilution) 5 ml of Luria broth (LB) media with NFZ (Sigma) at a concentration of 4 μg/ml. These cultures were incubated in dark at 37°C for 5 hr, followed by plating on LB agar at 1:20 dilutions in triplicates. The entire assay was repeated three times to ensure that the observations were reproducible.

ACCESSION NUMBERS

Coordinates and structure factors have been deposited in the PDB with accession numbers 4Q43 ($PolIV_{fdG:dCMPnPP}$), 4Q44 (PolIV-$fdGT1_{dA:dTMPnPP}$), and 4Q45 (PolIV-$fdGT3_{dA:dTMPnPP}$).

SUPPLEMENTAL INFORMATION

Supplemental Information includes Supplemental Results and eight figures and can be found with this article online at http://dx.doi.org/10.1016/j.str.2014.10.019.

AUTHOR CONTRIBUTIONS

D.T.N. designed and organized the study. J.K. purified PolIV and crystallized the three complexes. K.R.G., B.S., and P.I.P. synthesized the phosphoramidite for fdG and then synthesized and purified oligonucleotides containing the adduct. D.T.N. collected diffraction data. J.K. and A.S. together carried out structure determination, model building, and crystallographic refinement. J.K. carried out mutagenesis, purified the mutants, and carried out primer extension assays with WT and mutant protein. N.N. carried out the growth assays. A.S., J.K., and D.T.N. analyzed the data and wrote the manuscript, along with K.R.G., B.S., and P.I.P.

ACKNOWLEDGMENTS

We thank the X-ray diffraction facility located in the Molecular Biophysics Unit of the Indian Institute of Science. D.T.N. thanks Dr. Hassan Belrhali and Dr. Babu Manjashetty (BM14 beamline, ESRF) and Dr. Meitian Wang, Dr. Sandro Waltersperger, and Dr. Takashi Tomizaki (PXIII beamline, SLS). We also thank Dr. Claudia Höbartner (MPIbpc-Göttingen), as well as Prof. K.V.R Chary and Ms. Gitanjali A. Dhotre (TIFR-Mumbai) for providing ESI/MALDI spectra of oligos. The research was funded by NCBS-TIFR, RCB (D.T.N.) and DBT (P.I.P.). J.K. and A.S. are recipients of a Junior Research Fellowship (JRF) and a Senior Research Fellowship (SRF) from CSIR (government of India), respectively. K.R.G. was a recipient of an SRF from the University Grants Commission. N.N. is a recipient of a JRF from the ICMR. Data collection at the BM14 beamline of the ESRF (Grenoble, France) was funded by the BM14 project, a collaboration between DBT, EMBL, and ESRF.

Received: July 28, 2014
Revised: October 27, 2014
Accepted: October 28, 2014
Published: December 11, 2014

REFERENCES

Adams, P.D., Afonine, P.V., Bunkóczi, G., Chen, V.B., Davis, I.W., Echols, N., Headd, J.J., Hung, L.W., Kapral, G.J., Grosse-Kunstleve, R.W., et al. (2010). PHENIX: a comprehensive Python-based system for macromolecular structure solution. Acta Crystallogr. D Biol. Crystallogr. *66*, 213–221.

Bauer, J., Xing, G., Yagi, H., Sayer, J.M., Jerina, D.M., and Ling, H. (2007). A structural gap in Dpo4 supports mutagenic bypass of a major benzo[a]pyrene

dG adduct in DNA through template misalignment. Proc. Natl. Acad. Sci. U S A *104*, 14905–14910.

Benson, R.W., Norton, M.D., Lin, I., Du Comb, W.S., and Godoy, V.G. (2011). An active site aromatic triad in Escherichia coli DNA Pol IV coordinates cell survival and mutagenesis in different DNA damaging agents. PLoS ONE *6*, e19944.

Biertümpfel, C., Zhao, Y., Kondo, Y., Ramón-Maiques, S., Gregory, M., Lee, J.Y., Masutani, C., Lehmann, A.R., Hanaoka, F., and Yang, W. (2010). Structure and mechanism of human DNA polymerase eta. Nature *465*, 1044–1048.

Bot, C., Hall, B.S., Alvarez, G., Di Maio, R., González, M., Cerecetto, H., and Wilkinson, S.R. (2013). Evaluating 5-nitrofurans as trypanocidal agents. Antimicrob. Agents Chemother. *57*, 1638–1647.

Brünger, A.T., Adams, P.D., Clore, G.M., DeLano, W.L., Gros, P., Grosse-Kunstleve, R.W., Jiang, J.S., Kuszewski, J., Nilges, M., Pannu, N.S., et al. (1998). Crystallography & NMR system: a new software suite for macromolecular structure determination. Acta Crystallogr. D Biol. Crystallogr. *54*, 905–921.

Chandani, S., and Loechler, E.L. (2007). Molecular modeling benzo[a]pyrene N2-dG adducts in the two overlapping active sites of the Y-family DNA polymerase Dpo4. J. Mol. Graph. Model. *25*, 658–670.

Choi, J.Y., and Guengerich, F.P. (2005). Adduct size limits efficient and error-free bypass across bulky N2-guanine DNA lesions by human DNA polymerase eta. J. Mol. Biol. *352*, 72–90.

Choi, J.Y., and Guengerich, F.P. (2006). Kinetic evidence for inefficient and error-prone bypass across bulky N2-guanine DNA adducts by human DNA polymerase iota. J. Biol. Chem. *281*, 12315–12324.

Choi, J.Y., and Guengerich, F.P. (2008). Kinetic analysis of translesion synthesis opposite bulky N2- and O6-alkylguanine DNA adducts by human DNA polymerase REV1. J. Biol. Chem. *283*, 23645–23655.

Choi, J.Y., Angel, K.C., and Guengerich, F.P. (2006a). Translesion synthesis across bulky N2-alkyl guanine DNA adducts by human DNA polymerase kappa. J. Biol. Chem. *281*, 21062–21072.

Choi, J.Y., Stover, J.S., Angel, K.C., Chowdhury, G., Rizzo, C.J., and Guengerich, F.P. (2006b). Biochemical basis of genotoxicity of heterocyclic arylamine food mutagens: Human DNA polymerase eta selectively produces a two-base deletion in copying the N2-guanyl adduct of 2-amino-3-methylimidazo[4,5-f]quinoline but not the C8 adduct at the Narl G3 site. J. Biol. Chem. *281*, 25297–25306.

Choi, J.Y., Zang, H., Angel, K.C., Kozekov, I.D., Goodenough, A.K., Rizzo, C.J., and Guengerich, F.P. (2006c). Translesion synthesis across 1,N2-ethenoguanine by human DNA polymerases. Chem. Res. Toxicol. *19*, 879–886.

Cirz, R.T., and Romesberg, F.E. (2006). Induction and inhibition of ciprofloxacin resistance-conferring mutations in hypermutator bacteria. Antimicrob. Agents Chemother. *50*, 220–225.

Dipple, A. (1995). DNA adducts of chemical carcinogens. Carcinogenesis *16*, 437–441.

Editorial (2013). The antibiotic alarm. Nature *495*, 141.

Eoff, R.L., Choi, J.Y., and Guengerich, F.P. (2010). Mechanistic studies with DNA polymerases reveal complex outcomes following bypass of DNA damage. J. Nucleic Acids *2010*, 830473.

Foster, P.L. (2007). Stress-induced mutagenesis in bacteria. Crit. Rev. Biochem. Mol. Biol. *42*, 373–397.

Galhardo, R.S., Hastings, P.J., and Rosenberg, S.M. (2007). Mutation as a stress response and the regulation of evolvability. Crit. Rev. Biochem. Mol. Biol. *42*, 399–435.

Gore, K.R., Nair, D.T.; Pradeepkumar, P.I. (2013). Indian Patent Application 0454/MUM/2013, February 18, 2013.

Ikeda, M., Furukohri, A., Philippin, G., Loechler, E., Akiyama, M.T., Katayama, T., Fuchs, R.P., and Maki, H. (2014). DNA polymerase IV mediates efficient and quick recovery of replication forks stalled at N2-dG adducts. Nucleic Acids Res. *42*, 8461–8472.

Jarosz, D.F., Godoy, V.G., Delaney, J.C., Essigmann, J.M., and Walker, G.C. (2006). A single amino acid governs enhanced activity of DinB DNA polymerases on damaged templates. Nature *439*, 225–228.

Jarosz, D.F., Beuning, P.J., Cohen, S.E., and Walker, G.C. (2007). Y-family DNA polymerases in Escherichia coli. Trends Microbiol. *15*, 70–77.

Jarosz, D.F., Cohen, S.E., Delaney, J.C., Essigmann, J.M., and Walker, G.C. (2009). A DinB variant reveals diverse physiological consequences of incomplete TLS extension by a Y-family DNA polymerase. Proc. Natl. Acad. Sci. U S A *106*, 21137–21142.

Jia, L., Geacintov, N.E., and Broyde, S. (2008). The N-clasp of human DNA polymerase kappa promotes blockage or error-free bypass of adenine- or guanine-benzo[a]pyrenyl lesions. Nucleic Acids Res. *36*, 6571–6584.

Johnson, S.J., and Beese, L.S. (2004). Structures of mismatch replication errors observed in a DNA polymerase. Cell *116*, 803–816.

Johnson, J.R., Kuskowski, M.A., and Wilt, T.J. (2006). Systematic review: antimicrobial urinary catheters to prevent catheter-associated urinary tract infection in hospitalized patients. Ann. Intern. Med. *144*, 116–126.

Leslie, A.G.W., and Powell, H.R. (2007). Processing diffraction data with mosflm. In Evolving Methods for Macromolecular Crystallography, R.J. Read and J.L. Sussman, eds. (New York: Springer), pp. 41–51.

Levy, S.B., and Marshall, B. (2004). Antibacterial resistance worldwide: causes, challenges and responses. Nat. Med. *10* (12, Suppl), S122–S129.

Liu, Y., Yang, Y., Tang, T.S., Zhang, H., Wang, Z., Friedberg, E., Yang, W., and Guo, C. (2014). Variants of mouse DNA polymerase κ reveal a mechanism of efficient and accurate translesion synthesis past a benzo[a]pyrene dG adduct. Proc. Natl. Acad. Sci. U S A *111*, 1789–1794.

Lone, S., Townson, S.A., Uljon, S.N., Johnson, R.E., Brahma, A., Nair, D.T., Prakash, S., Prakash, L., and Aggarwal, A.K. (2007). Human DNA polymerase kappa encircles DNA: implications for mismatch extension and lesion bypass. Mol. Cell *25*, 601–614.

Lu, C., McCalla, D.R., and Bryant, D.W. (1979). Action of nitrofurans on E. coli: mutation and induction and repair of daughter-strand gaps in DNA. Mutat. Res. *67*, 133–144.

McCoy, A.J., Grosse-Kunstleve, R.W., Adams, P.D., Winn, M.D., Storoni, L.C., and Read, R.J. (2007). Phaser crystallographic software. J. Appl. Cryst. *40*, 658–674.

Minko, I.G., Washington, M.T., Prakash, L., Prakash, S., and Lloyd, R.S. (2001). Translesion DNA synthesis by yeast DNA polymerase eta on templates containing N2-guanine adducts of 1,3-butadiene metabolites. J. Biol. Chem. *276*, 2517–2522.

Nair, D.T., Johnson, R.E., Prakash, S., Prakash, L., and Aggarwal, A.K. (2004). Replication by human DNA polymerase-iota occurs by Hoogsteen base-pairing. Nature *430*, 377–380.

Nair, D.T., Johnson, R.E., Prakash, L., Prakash, S., and Aggarwal, A.K. (2005). Rev1 employs a novel mechanism of DNA synthesis using a protein template. Science *309*, 2219–2222.

Nair, D.T., Johnson, R.E., Prakash, L., Prakash, S., and Aggarwal, A.K. (2006). Hoogsteen base pair formation promotes synthesis opposite the 1,N6-ethenodeoxyadenosine lesion by human DNA polymerase iota. Nat. Struct. Mol. Biol. *13*, 619–625.

Nohmi, T. (2006). Environmental stress and lesion-bypass DNA polymerases. Annu. Rev. Microbiol. *60*, 231–253.

Pence, M.G., Blans, P., Zink, C.N., Hollis, T., Fishbein, J.C., and Perrino, F.W. (2009). Lesion bypass of N2-ethylguanine by human DNA polymerase iota. J. Biol. Chem. *284*, 1732–1740.

Pence, M.G., Blans, P., Zink, C.N., Fishbein, J.C., and Perrino, F.W. (2011). Bypass of N^2-ethylguanine by human DNA polymerase κ. DNA Repair (Amst.) *10*, 56–64.

Perrino, F.W., Harvey, S., Blans, P., Gelhaus, S., Lacourse, W.R., and Fishbein, J.C. (2005). Polymerization past the N2-isopropylguanine and the N6-isopropyladenine DNA lesions with the translesion synthesis DNA polymerases eta and iota and the replicative DNA polymerase alpha. Chem. Res. Toxicol. *18*, 1451–1461.

Petrosino, J.F., Galhardo, R.S., Morales, L.D., and Rosenberg, S.M. (2009). Stress-induced beta-lactam antibiotic resistance mutation and sequences of stationary-phase mutations in the Escherichia coli chromosome. J. Bacteriol. *191*, 5881–5889.

Rechkoblit, O., Malinina, L., Cheng, Y., Kuryavyi, V., Broyde, S., Geacintov, N.E., and Patel, D.J. (2006). Stepwise translocation of Dpo4 polymerase during error-free bypass of an oxoG lesion. PLoS Biol. *4*, e11.

Ryan, A., Kaplan, E., Laurieri, N., Lowe, E., and Sim, E. (2011). Activation of nitrofurazone by azoreductases: multiple activities in one enzyme. Sci Rep *1*, 63.

Seo, K.Y., Nagalingam, A., Miri, S., Yin, J., Chandani, S., Kolbanovskiy, A., Shastry, A., and Loechler, E.L. (2006). Mirror image stereoisomers of the major benzo[a]pyrene N2-dG adduct are bypassed by different lesion-bypass DNA polymerases in E. coli. DNA Repair (Amst.) *5*, 515–522.

Sharma, A., and Nair, D.T. (2012). MsDpo4-a DinB Homolog from Mycobacterium smegmatis-Is an Error-Prone DNA Polymerase That Can Promote G:T and T:G Mismatches. J. Nucleic Acids *2012*, 285481.

Sharma, A., Kottur, J., Narayanan, N., and Nair, D.T. (2013). A strategically located serine residue is critical for the mutator activity of DNA polymerase IV from Escherichia coli. Nucleic Acids Res. *41*, 5104–5114.

Shen, X., Sayer, J.M., Kroth, H., Ponten, I., O'Donnell, M., Woodgate, R., Jerina, D.M., and Goodman, M.F. (2002). Efficiency and accuracy of SOS-induced DNA polymerases replicating benzo[a]pyrene-7,8-diol 9,10-epoxide A and G adducts. J. Biol. Chem. *277*, 5265–5274.

Shrivastav, N., Fedeles, B.I., Li, D., Delaney, J.C., Frick, L.E., Foti, J.J., Walker, G.C., and Essigmann, J.M. (2014). A chemical genetics analysis of the roles of bypass polymerase DinB and DNA repair protein AlkB in processing N2-alkylguanine lesions in vivo. PLoS ONE *9*, e94716.

Silverstein, T.D., Jain, R., Johnson, R.E., Prakash, L., Prakash, S., and Aggarwal, A.K. (2010a). Structural basis for error-free replication of oxidatively damaged DNA by yeast DNA polymerase η. Structure *18*, 1463–1470.

Silverstein, T.D., Johnson, R.E., Jain, R., Prakash, L., Prakash, S., and Aggarwal, A.K. (2010b). Structural basis for the suppression of skin cancers by DNA polymerase eta. Nature *465*, 1039–1043.

Suzuki, N., Ohashi, E., Kolbanovskiy, A., Geacintov, N.E., Grollman, A.P., Ohmori, H., and Shibutani, S. (2002). Translesion synthesis by human DNA polymerase kappa on a DNA template containing a single stereoisomer of dG-(+)- or dG-(-)-anti-N(2)-BPDE (7,8-dihydroxy-anti-9,10-epoxy-7,8,9,10-tetrahydrobenzo[a]pyrene). Biochemistry *41*, 6100–6106.

Swan, M.K., Johnson, R.E., Prakash, L., Prakash, S., and Aggarwal, A.K. (2009). Structural basis of high-fidelity DNA synthesis by yeast DNA polymerase delta. Nat. Struct. Mol. Biol. *16*, 979–986.

Tangallapally, R.P., Yendapally, R., Daniels, A.J., Lee, R.E., and Lee, R.E. (2007). Nitrofurans as novel anti-tuberculosis agents: identification, development and evaluation. Curr. Top. Med. Chem. *7*, 509–526.

Taubes, G. (2008). The bacteria fight back. Science *321*, 356–361.

Walsh, J.M., Parasuram, R., Rajput, P.R., Rozners, E., Ondrechen, M.J., and Beuning, P.J. (2012). Effects of non-catalytic, distal amino acid residues on activity of E. coli DinB (DNA polymerase IV). Environ. Mol. Mutagen. *53*, 766–776.

Washington, M.T., Minko, I.G., Johnson, R.E., Haracska, L., Harris, T.M., Lloyd, R.S., Prakash, S., and Prakash, L. (2004). Efficient and error-free replication past a minor-groove N2-guanine adduct by the sequential action of yeast Rev1 and DNA polymerase zeta. Mol. Cell. Biol. *24*, 6900–6906.

Wolfle, W.T., Johnson, R.E., Minko, I.G., Lloyd, R.S., Prakash, S., and Prakash, L. (2006). Replication past a trans-4-hydroxynonenal minor-groove adduct by the sequential action of human DNA polymerases iota and kappa. Mol. Cell. Biol. *26*, 381–386.

Xu, P., Oum, L., Lee, Y.C., Geacintov, N.E., and Broyde, S. (2009). Visualizing sequence-governed nucleotide selectivities and mutagenic consequences through a replicative cycle: processing of a bulky carcinogen N2-dG lesion in a Y-family DNA polymerase. Biochemistry *48*, 4677–4690.

Yasui, M., Suzuki, N., Laxmi, Y.R.S., and Shibutani, S. (2006). Translesion synthesis past tamoxifen-derived DNA adducts by human DNA polymerases eta and kappa. Biochemistry *45*, 12167–12174.

Yasui, M., Suenaga, E., Koyama, N., Masutani, C., Hanaoka, F., Gruz, P., Shibutani, S., Nohmi, T., Hayashi, M., and Honma, M. (2008). Miscoding properties of 2′-deoxyinosine, a nitric oxide-derived DNA Adduct, during translesion synthesis catalyzed by human DNA polymerases. J. Mol. Biol. *377*, 1015–1023.

Yuan, B., Cao, H., Jiang, Y., Hong, H., and Wang, Y. (2008). Efficient and accurate bypass of N2-(1-carboxyethyl)-2′-deoxyguanosine by DinB DNA polymerase in vitro and in vivo. Proc. Natl. Acad. Sci. U S A *105*, 8679–8684.

Zang, H., Goodenough, A.K., Choi, J.Y., Irimia, A., Loukachevitch, L.V., Kozekov, I.D., Angel, K.C., Rizzo, C.J., Egli, M., and Guengerich, F.P. (2005). DNA adduct bypass polymerization by Sulfolobus solfataricus DNA polymerase Dpo4: analysis and crystal structures of multiple base pair substitution and frameshift products with the adduct 1,N2-ethenoguanine. J. Biol. Chem. *280*, 29750–29764.

Zhang, H., and Guengerich, F.P. (2010). Effect of N2-guanyl modifications on early steps in catalysis of polymerization by Sulfolobus solfataricus P2 DNA polymerase Dpo4 T239W. J. Mol. Biol. *395*, 1007–1018.

Zhang, Y., Wu, X., Guo, D., Rechkoblit, O., Geacintov, N.E., and Wang, Z. (2002). Two-step error-prone bypass of the (+)- and (-)-trans-anti-BPDE-N2-dG adducts by human DNA polymerases eta and kappa. Mutat. Res. *510*, 23–35.

Zhang, H., Eoff, R.L., Kozekov, I.D., Rizzo, C.J., Egli, M., and Guengerich, F.P. (2009a). Structure-function relationships in miscoding by Sulfolobus solfataricus DNA polymerase Dpo4: guanine N2,N2-dimethyl substitution produces inactive and miscoding polymerase complexes. J. Biol. Chem. *284*, 17687–17699.

Zhang, H., Eoff, R.L., Kozekov, I.D., Rizzo, C.J., Egli, M., and Guengerich, F.P. (2009b). Versatility of Y-family Sulfolobus solfataricus DNA polymerase Dpo4 in translesion synthesis past bulky N2-alkylguanine adducts. J. Biol. Chem. *284*, 3563–3576.

Zhao, B., Wang, J., Geacintov, N.E., and Wang, Z.G. (2006). Pol eta, Pol zeta and Rev1 together are required for G to T transversion mutations induced by the (+)- and (-)-trans-anti-BPDE-N-2-dG DNA adducts in yeast cells (vol 34, pg 417, 2006). Nucleic Acids Res. *34*, 1666.

Zhao, L., Christov, P.P., Kozekov, I.D., Pence, M.G., Pallan, P.S., Rizzo, C.J., Egli, M., and Guengerich, F.P. (2012a). Replication of N2,3-ethenoguanine by DNA polymerases. Angew. Chem. Int. Ed. Engl. *51*, 5466–5469.

Zhao, L., Pence, M.G., Christov, P.P., Wawrzak, Z., Choi, J.Y., Rizzo, C.J., Egli, M., and Guengerich, F.P. (2012b). Basis of miscoding of the DNA adduct N2,3-ethenoguanine by human Y-family DNA polymerases. J. Biol. Chem. *287*, 35516–35526.

Zorzi, R.R., Jorge, S.D., Palace-Berl, F., Pasqualoto, K.F., Bortolozzo, Lde.S., de Castro Siqueira, A.M., and Tavares, L.C. (2014). Exploring 5-nitrofuran derivatives against nosocomial pathogens: synthesis, antimicrobial activity and chemometric analysis. Bioorg. Med. Chem. *22*, 2844–2854.

Structure, Volume *23*

Supplemental Information

Unique Structural Features in DNA Polymerase IV Enable Efficient Bypass of the N^2 Adduct Induced by the Nitrofurazone Antibiotic

Jithesh Kottur, Amit Sharma, Kiran R. Gore, Naveen Narayanan, Biswajit Samanta, Pushpangadan I. Pradeepkumar, and Deepak T. Nair

Supplemental Results

A computational model of the $Dpo4_{fdG:dCTP}$ complex shows that the furfuryl moiety will clash with the enzyme residues and is buried in the fingers domain (Figure S6B). This result provides a rationale for the observation that the presence of minor groove N^2-adducts in the Dpo4 active site causes substantial distortion in the structure of substrate DNA and the enzyme (Figure S6C to S6I). Consequently, bypass of N^2-adducts by Dpo4 is considerably less efficient than synthesis on undamaged DNA. In the case of PolIV, the unique structural organization of the domains on binding to DNA allows minor groove N^2-adducts of dG to be accommodated within the active site with minimal change in structure.

The hydrophobic patch seen in the $PolIV_{fdG:dCMPnPP}$ structure is formed by the residues F13, I31, G32, G33, L71, L72, P73, G74, F76 and Y79 (Figure 5). The structurally equivalent residues in Dpo4 are Y12, V30, C31, G35, Y73, L74, P75, M76, K78 and Y81, respectively. The cavity occupied by the furfuryl moiety is absent in Dpo4 primarily because the residue equivalent to G74 in PolIV is M76 (Figure S7). In the case of Dpo4, a three residue insertion is present in the sequence corresponding to the hydrophobic patch and this leads to substantial differences in the local substructure and surface topology between Dpo4 and PolIV (Figure S7).

The PolIV-fdGT1dA:dTMPnPP structure was compared with the structures of Dpo4 with DNA containing the naphthyl-dG adduct at the T_1 position (2W8K and 2W8L). The Dpo4 structures exhibit substantial distortion for the adducted nucleotide (Figure S6C and S6D). A visual inspection of the enzyme surface of Dpo4 suggests that the finger-PAD channel in this enzyme is narrower than that in PolIV and there is no space towards the minor groove that can be occupied by the naphthyl adduct (Figure 4B and 4C).

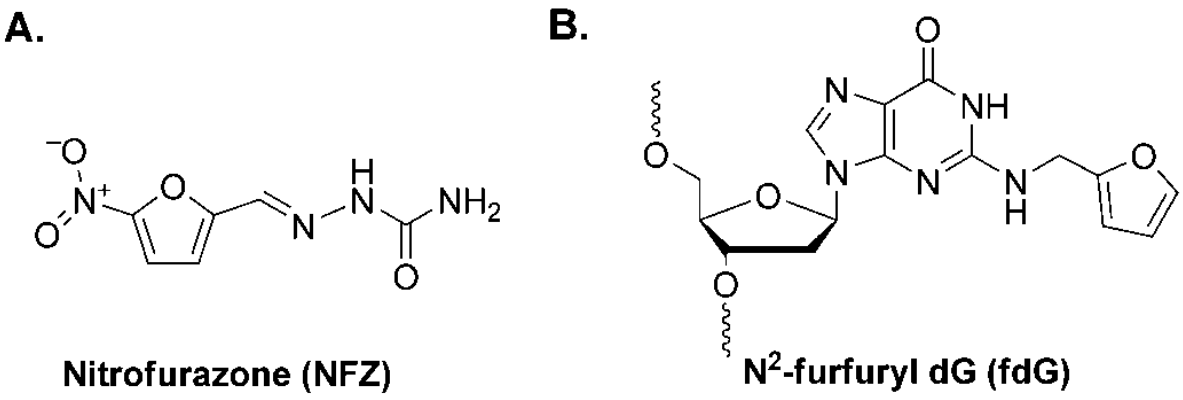

Figure S1, related to Experimental Procedures.Chemical structures of nitrofurazone (NFZ) antibiotic (A) and the N^2-furfuryldeoxyguanosine (fdG) adduct (B)

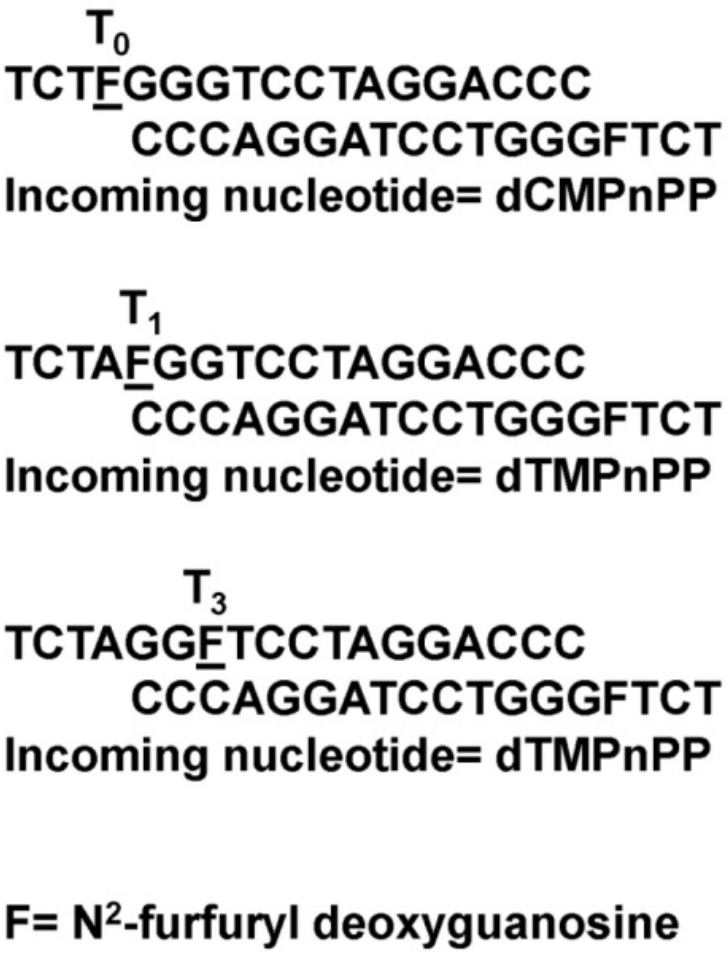

Figure S2, related to Experimental Procedures. DNA substrates used for crystallization. The DNA duplexes used for crystallization are displayed. The fdG adduct is present at T_0 (for incorporation), T_1 (for extension mode1) and T_3 (for extension mode2) in the three duplexes.

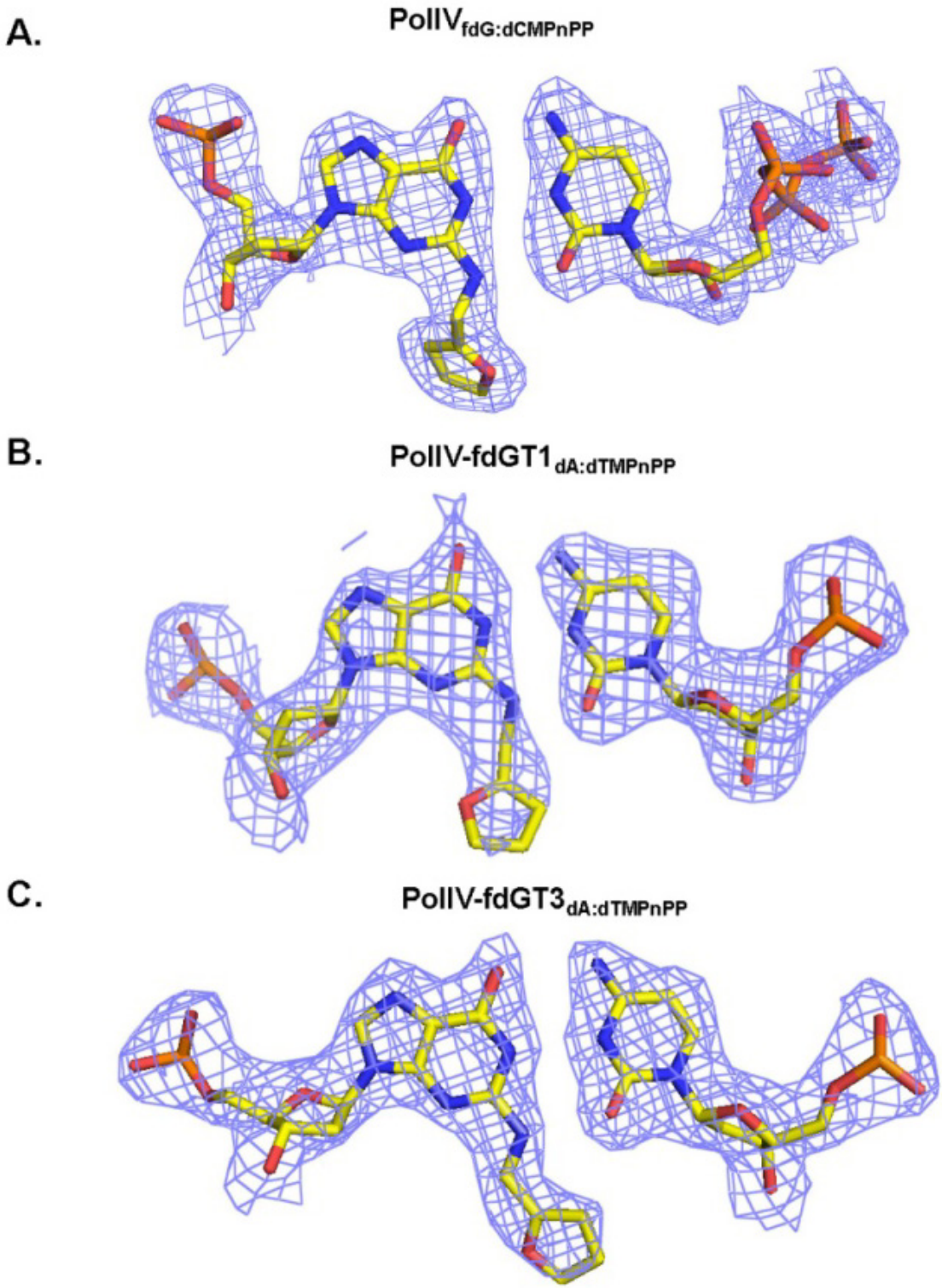

Figure S3, related to Figure 1. Electron Density maps for base pairs involving fdG. The electron density maps (2fo-fc) are displayed at a contour of 1.0 for base pairs involving fdG in the incorporation mode (A) and extension modes (B and C). (A) represents the incipient base pair (fdG:dCMPnPP) in the PolIV active site where as (B) and (C) exhibit base pairs (fdG:dC) that are part of the double-stranded region of the DNA substrate.

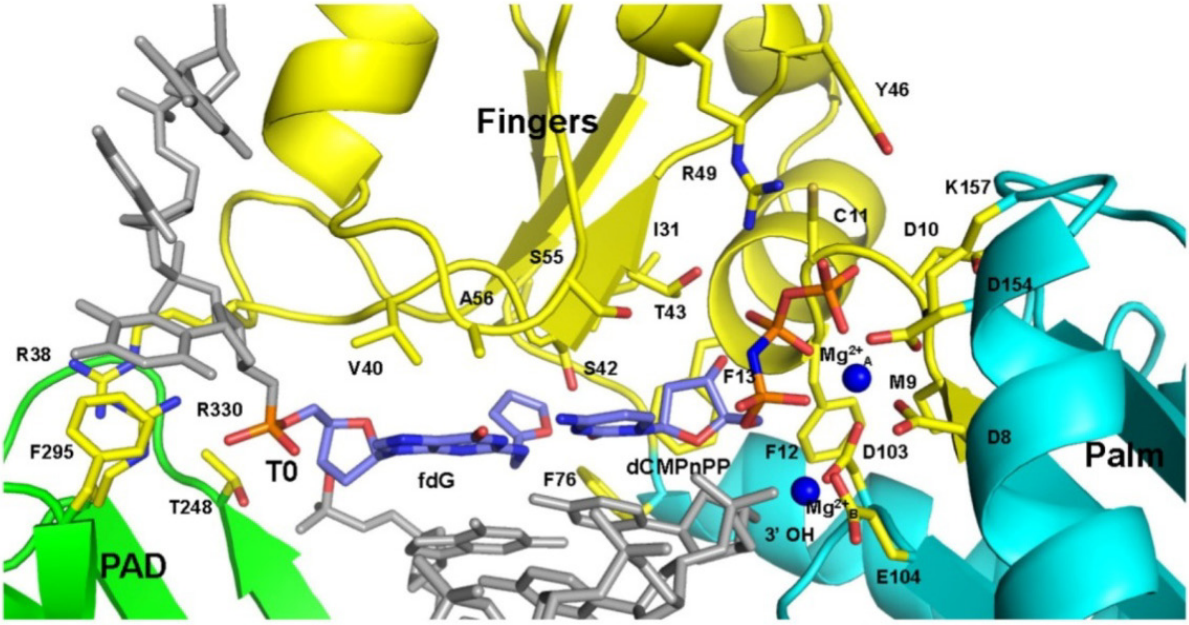

Figure S4, related to Figure 3. Active site in the PolIV$_{fdG:dCMPnPP}$ complex. The structure of the ternary complex is displayed in cartoon representation with the palm domain, fingers domain and the PAD region colored cyan, yellow and green, respectively. DNA is displayed in stick representation and grey color. The template and incoming nucleotide fdG and dCMPnPP are colored according to element. The magnesium ions are shown in the form of blue spheres. The residues of PolIV that interact with the template and incoming nucleotide are displayed in stick representation.

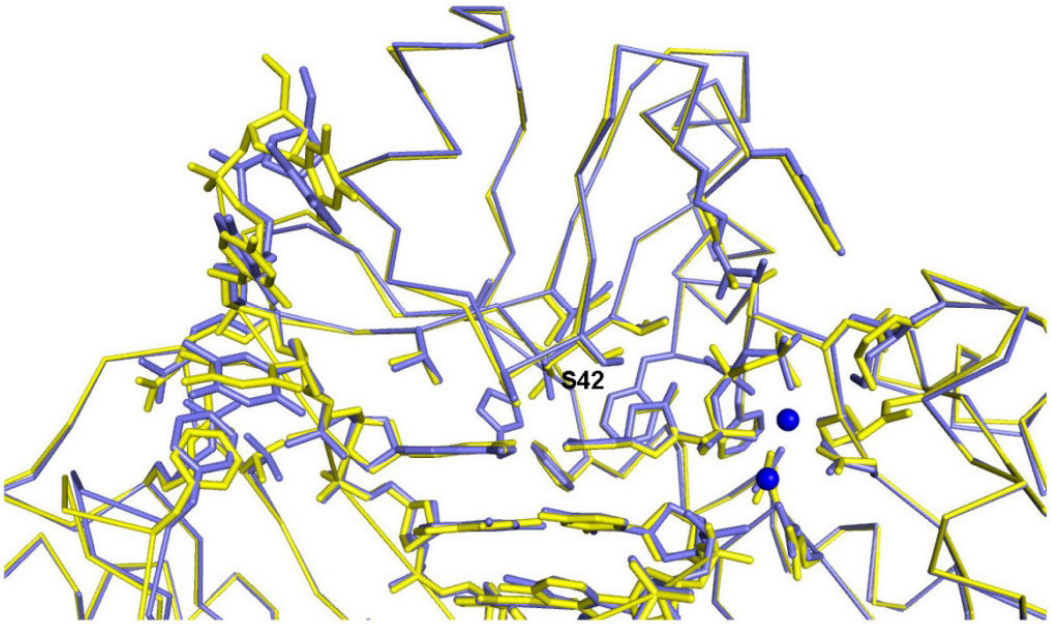

Figure S5, related to Figure 3. Comparison of the structure of $PolIV_{fdG:dCMPnPP}$ complex with that of $PolIV_{dG:dCMPnPP}$ (PDB code: 4IRC). The structural alignment of the two complexes is displayed. The $PolIV_{fdG:dCMPnPP}$ complex is colored slate and the $PolIV_{dG:dCMPnPP}$ is colored yellow. The backbone of the protein structure is presented in ribbon representation. The residues that interact with the incipient base pair in the two complexes, DNA substrate and dCMPnPP are displayed in stick representation and the Mg^{2+} ions are shown as blue spheres.

Template fdG

A.

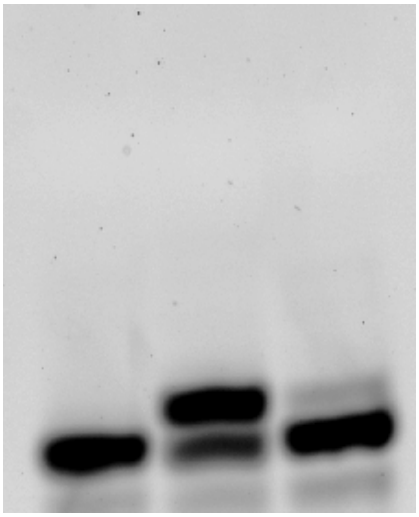

1 2 3

	Template fdG		
	1	2	3
PolIV	-	+	-
Dpo4	-	-	+
DNA (fdG)	+	+	+
dCTP	-	+	+
Mg^{2+}	-	+	+

B.

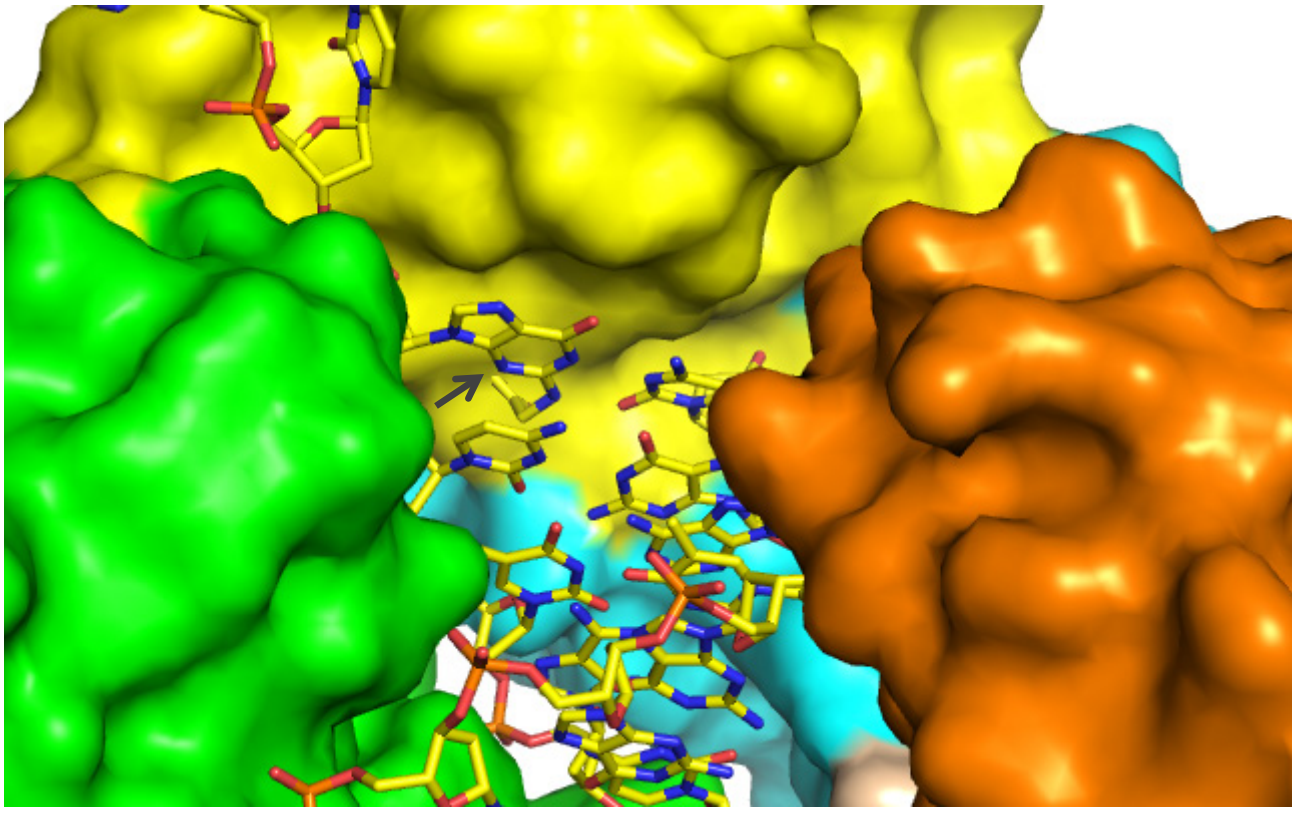

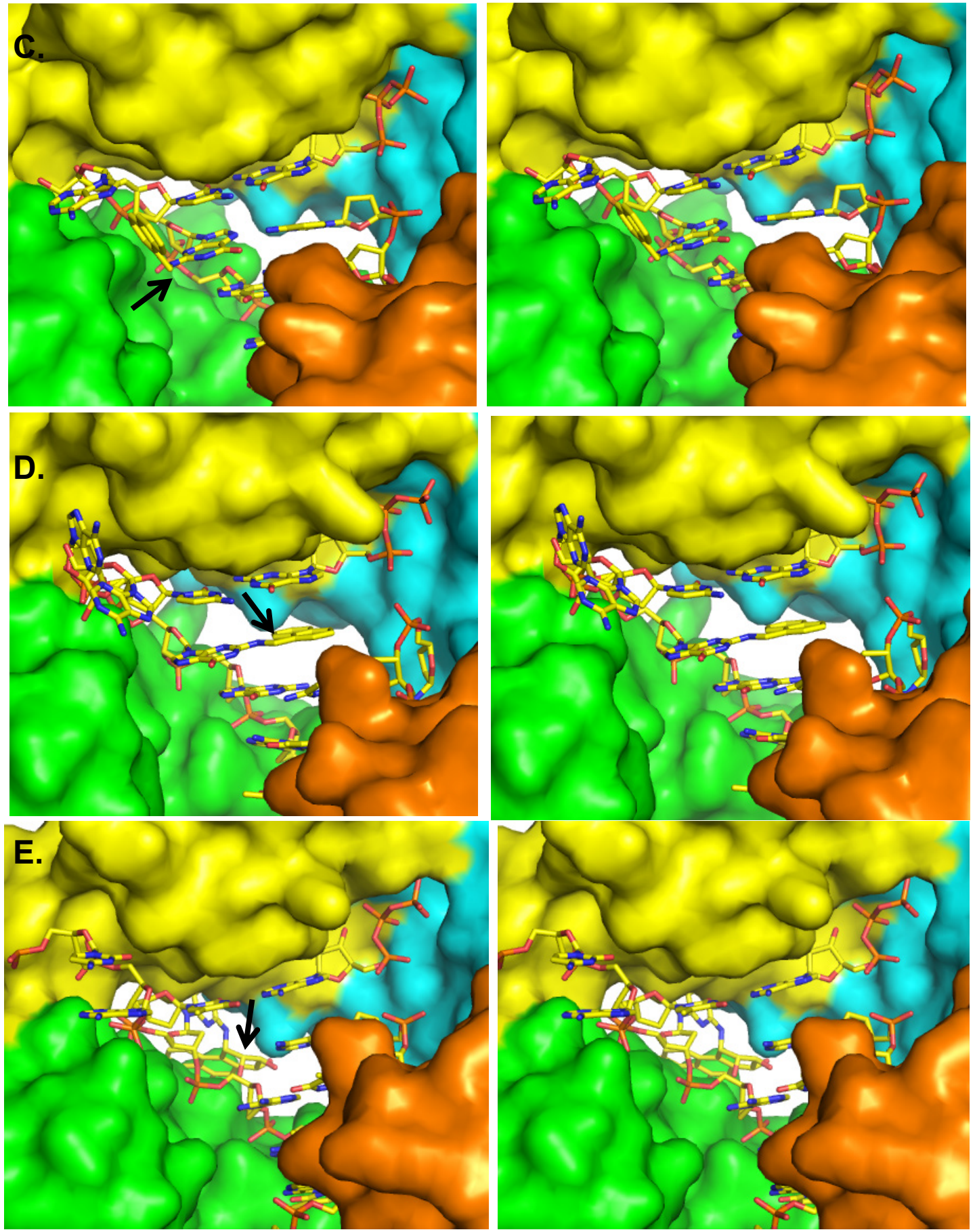
C.
D.
E.

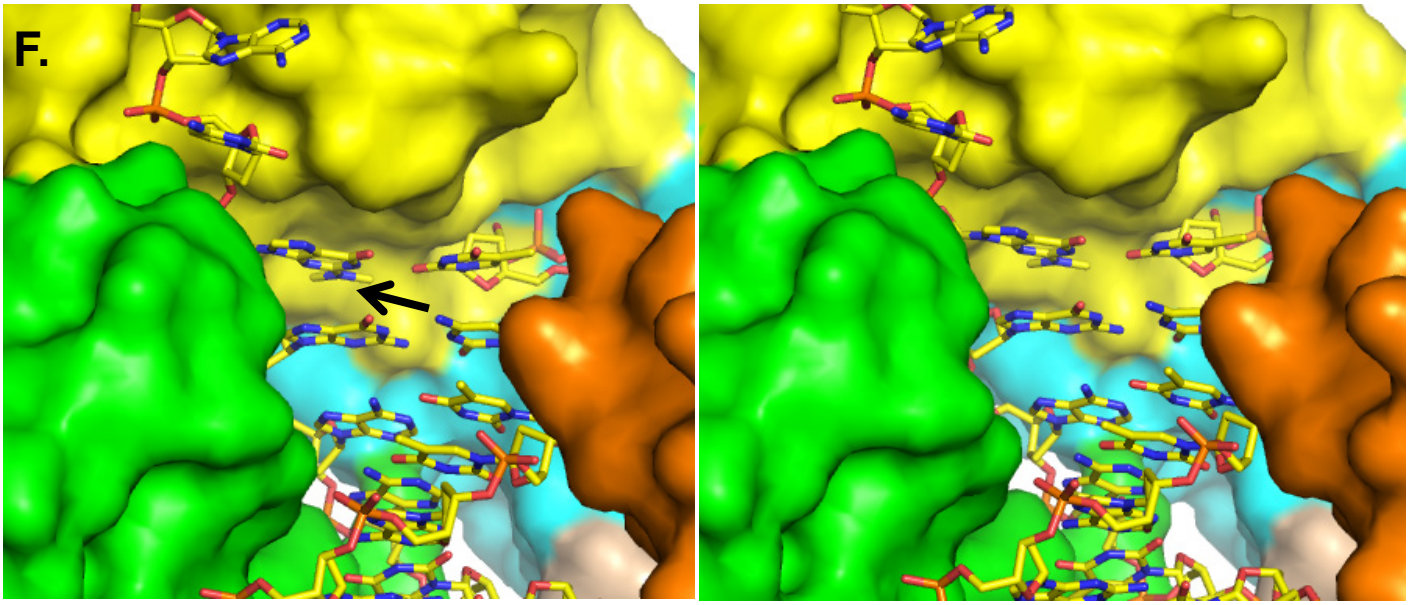
F.

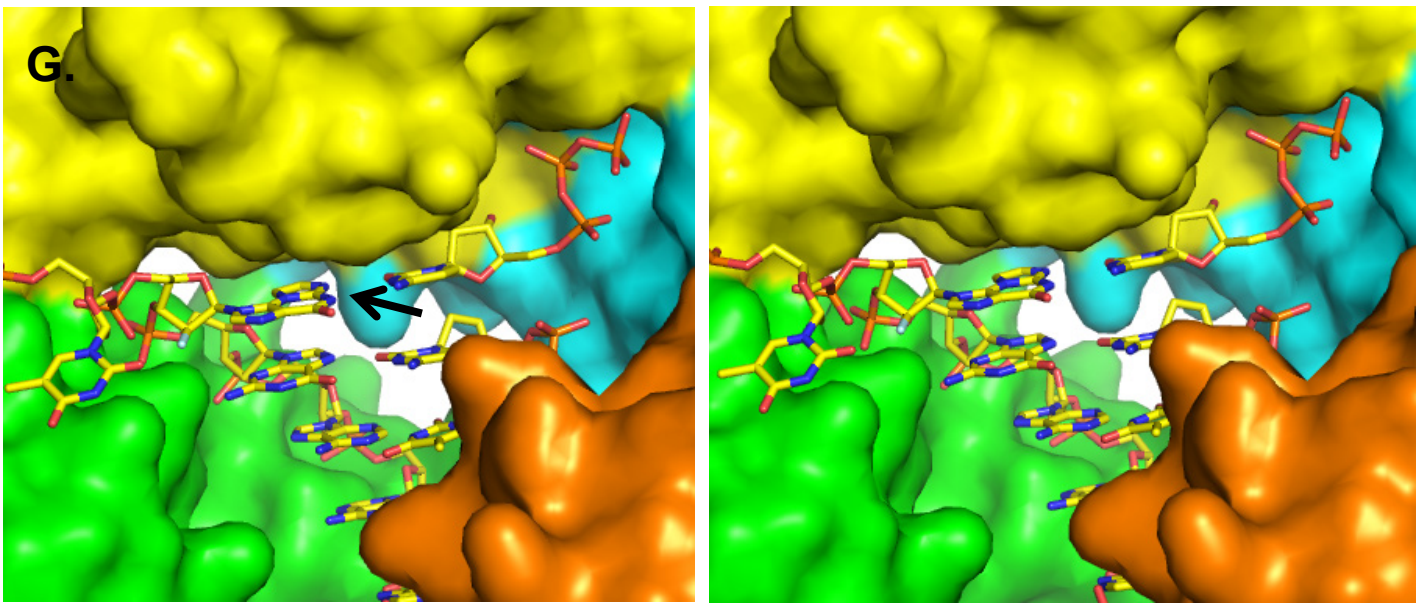
G.

Red: $Dpo4_{EdG:dCTP}$

Blue: $Dpo4_{dG:dCTP}$ (2ATL)

H.

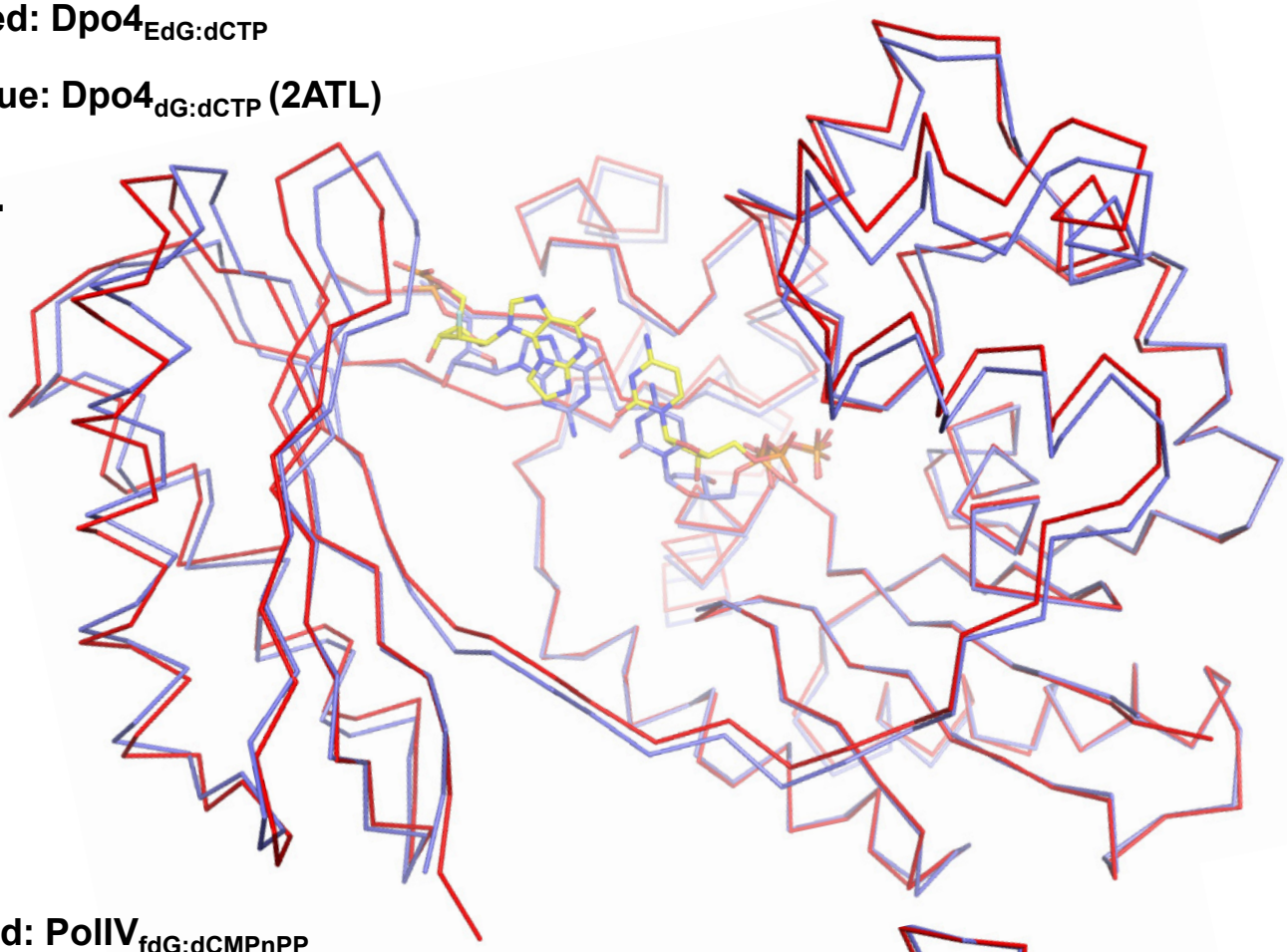

Red: $PolIV_{fdG:dCMPnPP}$

Blue: $PolIV_{dG:dCMPnPP}$ (4IRC)

I.

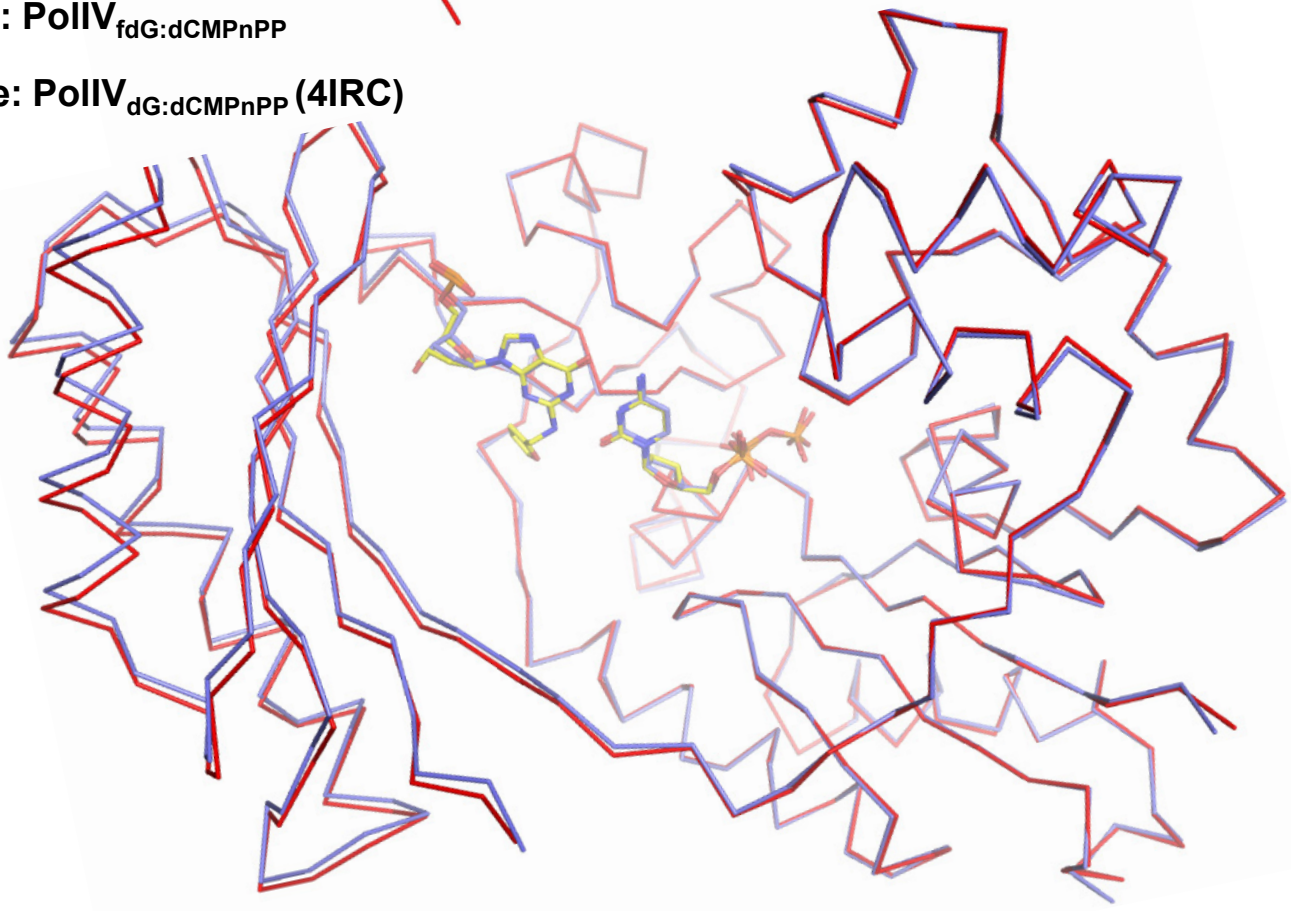

Figure S6, related to Figure 4. Comparison of bypass of N2-dG adducts by Dpo4 and PolIV. (A) fdG bypass by PolIV and Dpo4. The results for primer extension assay wherein wtPolIV (4 nM) and Dpo4 (4 nM) were incubated with fdG containing DNA duplexes (40 nM) and dCTP (5 μM) are displayed. The gel clearly shows that PolIV has much higher ability to incorporate dCTP opposite fdG than Dpo4. (B) Model of the $Dpo4_{fdG:dCTP}$ complex. A hypothetical model of the $Dpo4_{fdG:dCTP}$ complex is displayed here. The model was generated by superimposing the fdG nucleobase onto the guanine base of the template dG in the 2ATL structure. The arrow shows the position of fdG residue. The model shows that the furfuryl ring is buried in the fingers domain and will clash with the enzyme residues present towards the minor groove of the fdG adduct. The model suggests that significant distortions in enzyme and DNA structure may be required to accommodate the furfuryl adduct in the Dpo4 active site and this may be responsible for the significantly lower ability of Dpo4 to bypass the fdG adduct as compared to PolIV.

Minor groove N^2-adducts exhibits a diversity of conformations in the Dpo4 active. Stereo figures of close-ups of the active site of Dpo4 in complex with DNA containing different minor groove N^2-adducts of varying sizes and chemical nature are displayed. The adducts include N^2-naphthyl (C& D), Benzopyrene diol epoxide (E), N^2,N^2-dimethyl adduct (F) and N^2-3-ethenoguanine adduct (G). The adducts are marked by arrows for clarity.

The incipient base pairs in complexes of Dpo4 and PolIV with undamaged and damaged DNA were compared. The structure of Dpo4 in complex with DNA containing the N^2, 3-ethenoguanine (N2EdG) adduct base paired with dCTP is available (3V6J). The alignment of the structures of Dpo4 in complex with undamaged (2ATL) and damaged (N2EdG) DNA are displayed (H). The alignment shows that there are differences in the positioning of the incipient base pairs in the enzyme active site. The adducted guanine occupies a raised position presumably to avoid clashes between the etheno- ring and the enzyme residues. A similar alignment for PolIV is also displayed wherein the damaged template base is the fdG adduct (I). This alignment shows that the two base pairs overlap and there is minimal change in the positioning of nascent base pair. Thus, PolIV can accommodate the larger fdG adduct in the enzyme active site without any distortion in the incipient base pair.

A.

```
PolIV   4    IIHVDMDCFFAAVEMRDNPALRDIPIAI---GGSRERRGVISTANYPARKFGVRSAMPTG  60
Dpo4    3    VLFVDFDYFYAQVEEVLNPSLKGKPVVVCVFSGRFEDSGAVATANYEARKFGVKAGIPIV  62
                          *
PolIV   61   MALKLCPHLTLLPGRFDAYKEASNHIREIFSRYTSRIEPLSLDEAYLDVTDSVHCHGSAT  120
Dpo4    63   EAKKILPNAVYLPMRKEVYQQVSSRIMNLLREYSEKIEIASIDEAYLDISDKVRDYREAY  122

PolIV   121  LIAQEIRQTIFNELQLTASAGVAPVKFLAKIASDMNKPNGQFVITPAEVPAFLQTLPLAK  180
Dpo4    123  NLGLEIKNKILEKEKITVTVGISKNKVFAKIAADMAKPNGIKVIDDEEVKRLIRELDIAD  182

PolIV   181  IPGVGKVSAAKLEAMGLRTCGDVQKCDLVMLLKRFGKFGRILWERSQGIDERDVN-SERL  239
Dpo4    183  VPGIGNITAEKLKKLGINKLVDTLSIEFDKLKGMIGE-AKAKYLISLARDEYNEPIRTRV  241

PolIV   240  RKSVGVERTMAEDIHHWSECEAI----IERLYPELERRLAK------VKPDLLIARQG    287
Dpo4    242  RKSIGRIVTMKRNSRNLEEIKPYLFRAIEESYYKLDKRIPKAIHVVAVTEDLDIVSRG    299
```

B.

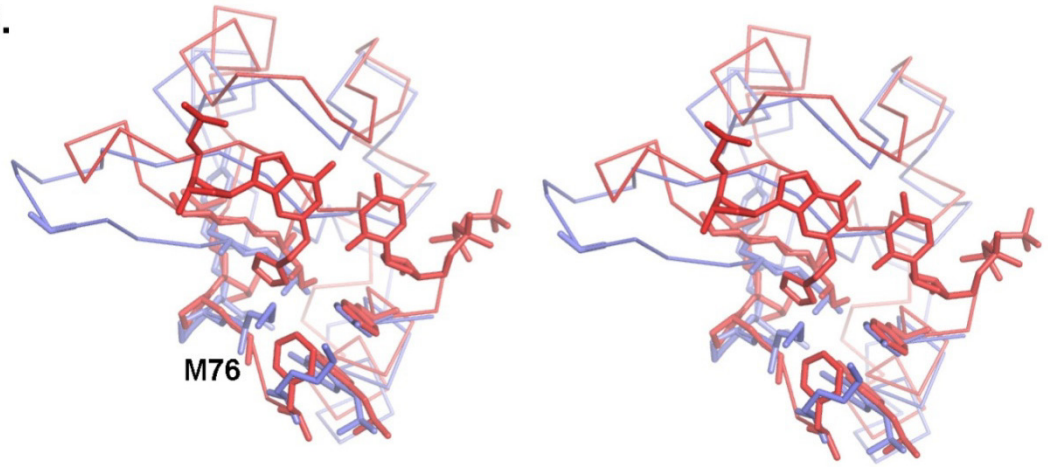

Red: PolIV$_{fdG:dCMPnPP}$

Blue: Dpo4$_{dG:dCTP}$ (2ATL)

Figure S7, related to Figure 5. Comparison of the residues that contribute to the formation of hydrophobic patch on the enzyme surface. (A) The sequence alignment of Dpo4 and PolIV is displayed and the residues that form the hydrophobic patch on the fingers domain are highlighted by a yellow background. In the case of PolIV, there is a three residue deletion in a stretch of sequence that contributes to the formation of the hydrophobic patch. Additionally, the difference G74(PolIV)→M76(Dpo4) is highlighted by an asterisk sign in the alignment. (B) A stereo figure of the alignment of the fingers domain from PolIV$_{fdG:dCMPnPP}$ and 2ATL is displayed. The residues that form the hydrophobic patch- highlighted in the alignment- are displayed in stick representation along with the fdG:dCMPnPP base pair. The M76 residue of Dpo4 is labeled as the side chain of this residue will clash with the furfuryl ring of the fdG adduct.

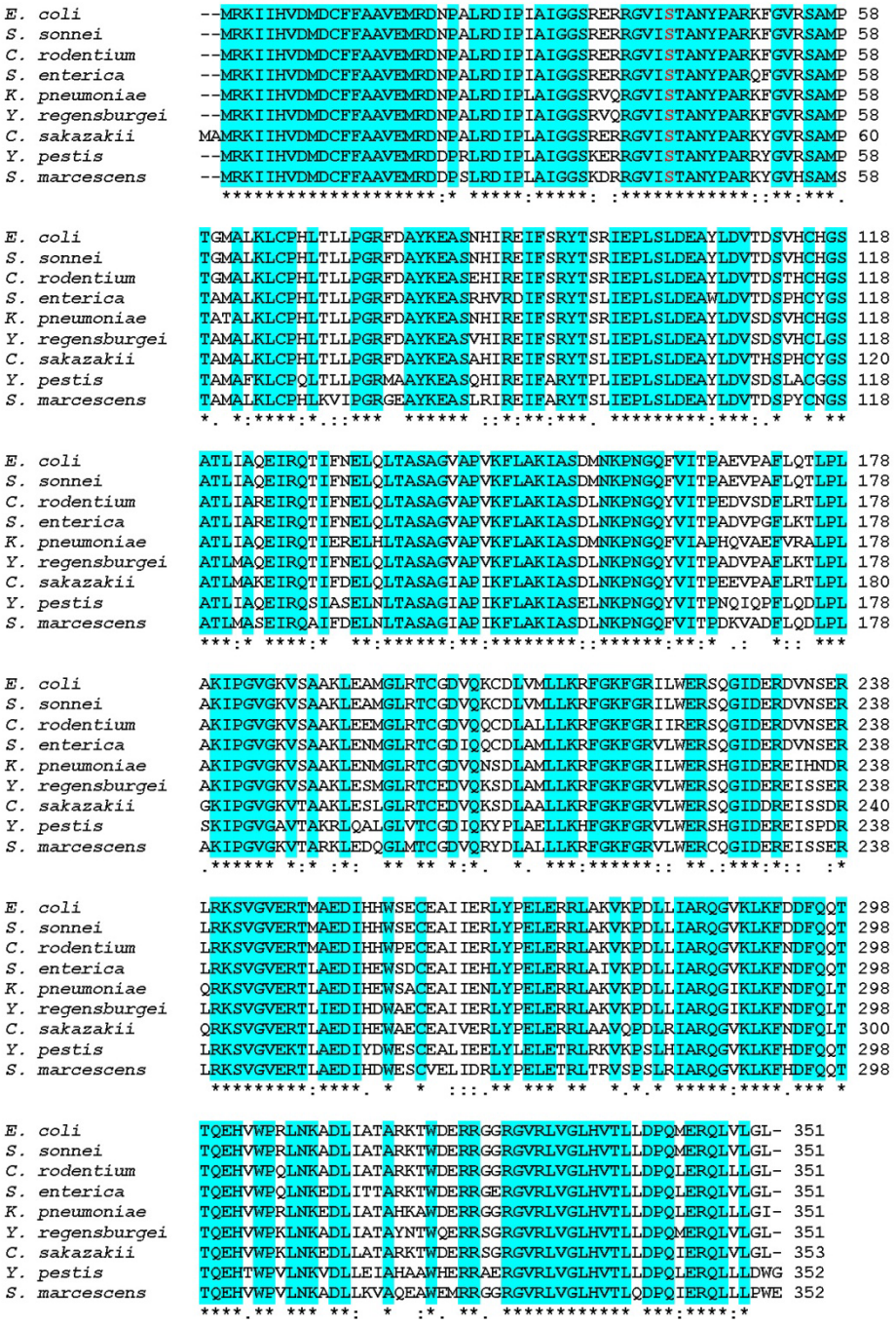

Figure S8, related to Figure 6. Sequence alignment of orthologs of PolIV. The alignment of the orthologs of PolIV from different pathogenic bacteria is displayed. The residues that are identical in all the displayed orthologs are highlighted by cyan background. PolIV (*Escherichia coli*) exhibits high sequence identity with orthologs from *Shigella sonnei* (100%), *Citrobacter rodentium* (95%), *Salmonella enterica* (92%), *Klebsiella pneumoniae* (89%), *Yokenella regensburgei* (91%), *Cronobacter sakazakii* (88%), *Yersinia pestis* (79%) and *Serratia marcescens* (74%).